SGG SGS sc | nat
Swiss Journal of Geosciences

ORIGINAL PAPER Open Access

Coupling length: a generalized gleno-acetabular distance measurement for interpreting the size and gait of quadrupedal trackmakers

Kent A. Stevens[1*], Scott Ernst[2] and Daniel Marty[3]

Abstract

The gleno-acetabular distance D_{GA}, a conventional proxy for the size of a quadrupedal trackmaker, is often estimated as the distance GA between the midpoint between a left and right pair of pes tracks and the midpoint between a selected pair of left and right manus tracks. While frequently used to estimate trackmaker size from fossil trackways, the relationship between GA and D_{GA} depends upon the gait (which is unknown for extinct trackmakers), and is subject to multiple additional sources of uncertainty including which specific pair of manus tracks to associate with a given pair of pes tracks. Here a generalization is introduced, termed coupling length, which does not require any presumption about trackmaker gait of the degree of overstepping. On the contrary, a systematic analysis of a trackway in terms of coupling length can permit estimation of both the size and the gait with which the trackmaker progressed. Coupling length can be computed at successive points along a trackway, allowing exploration of a range of hypothetical gaits and body sizes for the trackmaker responsible. A fitness function quantifying persistent variation in coupling length along a trackway is used to indicate whether a given trackway could have been created by a fairly consistent gait, and if so, a range of high-fitness solution gaits and their associated D_{GA}. The method was applied to selected quasi-regular sauropod trackways and a solution found for a narrow range of gaits with limb phase of about 0.3 and $D_{GA} = 1.6 \pm 0.2$ m. This is the first estimation of sauropod trackmaker gait, and introduces a novel method by which irregularity along a trackway is used as a source of information to constrain inferences of trackmaker behavior. The computed D_{GA} for this sauropod suggests significantly smaller trackmakers than conventional estimations based on track dimensions and hip height estimates. Size estimation by this approach offers greatly reduced uncertainty compared to conventional estimates.

Keywords: Locomotion, Trackway analysis, Gait analysis, Quadrupedal size, Trackmaker identification, Quantitative ichnology, Gleno-acetabular distance

1 Introduction

1.1 Summary

An extensive collection of sauropod trackways uncovered near Porrentruy in the Canton Jura (NW Switzerland) provided a rich dataset of thousands of well-preserved sauropod tracks, comprising about 260 trackways, many of which extended over hundreds of meters (Marty, 2008; Marty et al., 2003, 2004, 2010). A thorough statistical analysis was performed, which led to a novel

Editorial handling: Michael Benton.

*Correspondence: kent@cs.uoregon.edu
[1] Department of Computer and Information Science, University of Oregon, Eugene, OR 97403, USA
Full list of author information is available at the end of the article

probabilistic method whereby variations in nearly-regular trackway yielded inferences about the size and gait of the now-extinct trackmakers. The method is offered as a refinement of the conventional approach to gleno-acetabular distance estimation, but it is restricted to gaits with duty factors greater than 0.5, and presumes the trackmaker was engaged in a symmetrical gait. This approach was documented in the final report on these ichnoassemblages (Paratte et al., 2018; Stevens & Ernst, 2017); see also (Stevens et al., 2017), wherein we reported upon this statistically-independent method for estimating trackmaker size (gleno-acetabular length) that is in close agreement with the estimate provided by conventional heuristics, but with finer numerical precision. The method simultaneously solved for the sauropod's gait and suggested a narrow range of limb phases spanning about 0.25–0.3 (i.e., from a lateral sequence singlefoot to a lateral sequence diagonal couplet) (Stevens et al., 2017). The method presumes the use of explicit estimates of track measurement uncertainty (Paratte et al., 2018; Stevens & Ernst, 2017). The uncertainty in localizing tracks along a trackway imposes practical limits on the precision with which gait can be inferred.

1.2 Conventional methods for estimating trackmaker size

As a quadruped traverses a substrate that preserves its passage, the two forelimbs form a succession of manus tracks which is soon followed by the pes tracks created by the two hindlimbs. A regular, constant gait results in a repeating pattern of interleaved pes and manus tracks, the spacing and arrangement of which depending upon the separation between the forelimb pair and the hindlimb pair, the length of the steps it takes, and the relative timing of the placement of the four limbs (i.e., the gait). An important goal of trackway interpretation, especially for fossil trackways, is the inference of those properties of the trackmaker from measurements of the trackway. In the absence of the (now extinct) trackmaker, the inferences are grounded variously by analogy with the proportions, kinematics, dynamics, and behaviors of extant trackmakers. A few of the most common inferences attempt to rather directly relate trackway measurements to corresponding trackmaker measurements, relying on assumed constants of proportionality, heuristics about the gait that creates a given track pattern, and other rules of thumb. The more assumptions required of a given method, the more uncertain are the predictions it provides.

There are two conventional approaches towards trackmaker estimation from fossil trackways: track-based and trackway-based. The track-based approach estimates trackmaker hip height H_A from measured pes track length PL (or pes width PW), based on a presumed linear relationship ratio H_A/PL (or H_A/PW). Inferred hip height is then used to estimate trackmaker size (e.g., gleno-acetabular distance D_{GA}) based on another presumed linear proportionality (D_{GA}/H_A) and estimated hip height is also used to estimate trackmaker speed based on other heuristics (e.g., Alexander, 1976; Lockley, 1991; Thulborn, 1990)—see Eq. 1, below. Estimated hip height, size, and speed are obviously subject to the uncertainty associated with those unknown proportionality constants, the validity of assuming linear proportionality in body dimensions (which disregards allometry and relies on assumptions about the ichnotaxon), and the measurement uncertainty. We consider the degree of uncertainty associated with such track-based assumptions in the discussion.

Alternatively, the conventional trackway-based approach estimates the separation between the pectoral and pelvic girdles by measuring their so-called "manus-pes" distance (e.g., Leonardi, 1987). In Fig. 1, a pair of manus tracks {LM2, RM2} is assumed to correspond to the locations of the forelimbs when the hindlimbs correspond to the pes tracks {LP1, RP1}. Each pair of tracks is connected by a line segment, the midpoint of which would indicate the center of the corresponding girdle. Those midpoints are then connected by a line segment GA. The length of GA (the "manus-pes distance") would presumably correspond to D_{GA} for a trackmaker standing stationary in those four tracks, or in location provided the gait has an interval in which all four limbs are simultaneously in support phase. The gait, however, is unknown, and while some gaits such as a trot do have such an interval during the step cycle, many quadrupedal gaits have a maximum of only three limbs in support (Hildebrand, 1965, 1976). Alternative formulae have thus been proposed that add a heuristic correction factor such as "half the stride length plus the manus-pes distance", or "about three-quarters the stride length plus the manus-pes distance", "plus one or two stride lengths to the body lengths depending on the degree of overlap" (Demathieu, 1970; Farlow et al., 1989; Halfpenny, 1987; Leonardi, 1987; Padian & Olsen, 1984). Clearly a heuristic that adds as much as three-quarters of a stride length to account for the unknown gait, plus perhaps one or two integral stride lengths to account for the hypothesized degree of overlap, adds considerable uncertainty to the estimate.

A source of greater uncertainty is the choice of manus tracks to associate with a given pair of pes tracks (Leonardi, 1987; Peabody, 1959). In Fig. 1, instead of choosing the manus pair {LM2, RM2} as diagrammed, the manus pair {LM1, RM1} were selected, GA would be implausibly short, but another choice possible pairs of manus tracks such as {LM3, RM3} cannot be ruled out a priori, and would suggest a body length a full stride length longer. Other sources of uncertainty can be identified, such the

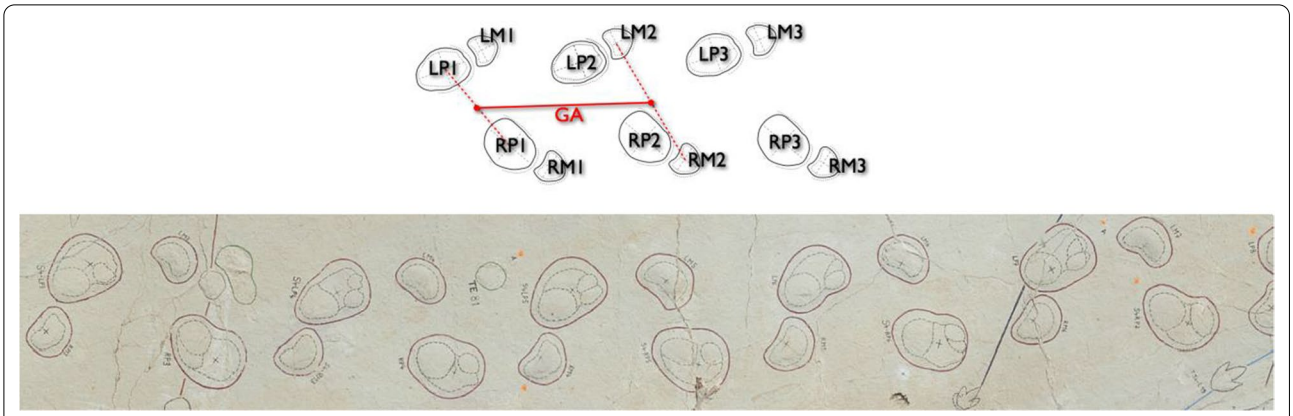

Fig. 1 In the conventional practice of quadrupedal trackmaker size estimation, a line segment is constructed between two pes tracks (LP1 and RP1, above) and another between two manus tracks (LM2 and RM2). The separation GA between the centers of these two line segments is often used as the basis for estimating the trackmaker's gleno-acetabular distance D_{GA}, subject to a correction to account for the presumed gait (see text), and having selected the correct pair of manus tracks to associate with the given pair of pes tracks. Perhaps contrary to intuition, an exquisitely preserved and regular trackway such as BEB-500-S4 (lower), one of the trackways used in this study, could have been created by a quadruped of many possible sizes and many possible gaits

unknown degree of lateral flexion of the vertebral column during a step cycle, and differences in the amount of limb protraction versus retraction, as occurs in crouched or sprawling animals (Bonnan et al., 2016; Fischer et al., 2002; Irschick & Jayne, 1999). Finally, there is uncertainty in an estimate that arises from basic measurement error, such as locating track centers. While measurement error in this case is minor compared to other sources of uncertainty just mentioned, the compounding of uncertainty in nontrivial mathematical computations, so-called error propagation (Taylor, 1997), will be demonstrated to be a limiting factor in the current study, and has perhaps an under-appreciated importance to quantitative ichnology in general.

The current study provides an alternative to the conventional track- and trackway-based approaches. Our analysis, by design, makes only minimal assumptions about the trackmaker. It does not presume any heuristic coefficients to scale hip height or body length; it also does not presume the trackmaker was engaged in any particular gait, other than it being a symmetrical and without an aerial phase, as will be discussed further). It relies on selecting a sufficiently regular and complete segment of a trackway, and while we make no assumption about gait or body size, we presume that the trackmaker maintained an approximately constant gait and body length D_{GA}. We then search through a space of possible solutions for a schematic trackmaker to the given track position data and select that solution (or set of similar solutions) that minimizes the apparent variation in body length. As will be shown, however, even with regular trackways and excellent track preservation, error propagation that starts with an inevitable degree of trackway measurement uncertainty becomes one of the most significant factors that limits the estimation of body size and the inference of the gait that best accounts for the given trackway pattern.

While this study was devised specifically for sauropod dinosaur trackway interpretation, it is not narrowly restricted to sauropods, and while the methods we present have yet to be applied to extant quadrupeds for empirical validation, we are able to show that this novel method provides an independent means for the sort of trackmaker estimates that are often made based on a few static measurements of track dimensions and the separations between successive tracks.

1.3 Limb phase and duty factor

In a regular quadrupedal gait, the four limbs maintain a fixed relative timing of footfalls. We will refer to the left and right manus as M_L and M_R and the left and right pes as P_L and P_R, and we adopt the conventional formulation where a step cycle begins when the left pes just contacts the ground (Hildebrand, 1965, 1976, 1989). The start of the support for the other three limbs is thus measured relative to $P_L = 0$. The fraction of the step cycle that each limb remains in contact (or support) is the duty factor DF (or duty cycle). This study presumes $DF > 0.5$, hence at least three limbs are simultaneously in support at any time throughout the step cycle. Additionally, we presume the duty factor for the forelimbs and hindlimbs are identical. Moreover, in this study we are concerned with symmetrical regular gaits, i.e., gaits in which the contralateral limbs are out of phase by one half cycle, therefore the

relative timing of the footfalls for all four limbs for a regular gait can be characterized by a single parameter, limb phase *LP*, the relative fraction ($0 \le LP \le 1.0$) of a complete step cycle of the footfall for M_L. The four gaits pace, walk, trot, and amble are separated by 0.25 in limb phase (see Fig. 2). The pace ($LP = 0.0$) corresponds to the left forelimb and hindlimb moving together in synchrony, and in counterphase relative to the right forelimb and hindlimb. In a trot ($LP = 0.5$) the left forelimb and the right hindlimb in synchrony and in counterphase with the right forelimb and left hindlimb. A walk ($LP = 0.25$), which is intermediate between a pace and a trot, is a 'lateral sequence singlefoot', so named as the next footfall after the left hind limb is on the same side, and only one foot touches down at a time (Hildebrand, 1965).

Between the pace and the walk is an intermediate gait ($LP = 0.125$), a 'lateral-sequence lateral-couplet' gait favored by dogs engaged in walking at a steady speed (Griffin et al., 2004). Likewise, between the walk and the trot is an intermediate gait ($LP = 0.375$), a 'lateral-sequence diagonal-couplet' that is sometimes called the '4-beat trot', or 'trot-like walk' or even 'dirty' trot (Lammers & Biknevicius, 2004; Reilly & Biknevicius, 2003; Zips et al., 2001). To include these four intermediate gaits for a total of eight gaits, we use a simple numbering convention *G0*–*G7* (see Table 1).

While there is universal understanding of 'pace', 'walk', and 'trot' (sensu Hildebrand, 1965), a 'walking' gait can also refer to any gait that uses inverted-pendulum (vaulting) mechanics as opposed to a 'running' gait that uses bounding (bouncing) mechanics (Biknevicius & Reilly, 2006; Cavagna et al., 1977). A naming quagmire has thus resulted, wherein "*... some gaits are theoretically possible as both walks and runs (trots and singlefoots) whereas other gaits occur primarily as runs (pace) or as walks (all other symmetrical gaits)*" (Biknevicius & Reilly, 2006). Since a trot (as traditionally defined by the footfall pattern) might also be either a walk or a run based on its whole-body dynamics, we will follow the restricted usage of these gait terms to only describe footfall patterns as suggested by Biknevicius and Reilly (2006). There is still a matter of how to refer to the four intermediate gaits (*G1*, *G3*, *G5*, and *G7*) in a way that reflects their footfall patterns. The *G1* gait is referred to here as a 'pacing walk' as it is intermediate between a pace and a walk, and similarly *G3* is a 'walking trot' as it is intermediate between a walk and a trot, and essentially a diagonal-couplet.

The literature also has some potential confusion in the use of the term 'amble'. An amble can be either a diagonal sequence gait *G6* ($LP = 0.75$) or a lateral sequence gait

Table 1 Gaits are conventionally defined by the timing of the footfall pattern

Limb phase	Gait	Abbreviation	Sequence	Couplets
0.0	Pace	*G0*	Lateral	Lateral
0.125	'Pacing Walk'	*G1*	Lateral	Lateral
0.25	Walk	*G2*	Lateral	Singlefoot
0.375	'Walking Trot'	*G3*	Lateral	Diagonal
0.5	Trot	*G4*	Diagonal	Diagonal
0.625	'Trotting Amble'	*G5*	Diagonal	Diagonal
0.75	Amble	*G6*	Diagonal	Singlefoot
0.875	'Ambling Pace'	*G7*	Diagonal	Lateral

A step cycle can be regarded as starting with the left pes beginning the support phase. For symmetrical gaits, the left and right hindlimbs P_L and P_R are out of phase by 0.5, as are M_L relative to M_R. Limb phase refers to the fraction of the cycle at which the left manus M_L begins its support for the left pes P_L. Four additional intermediate gaits are included to provide a denser sampling of this continuum for our analysis

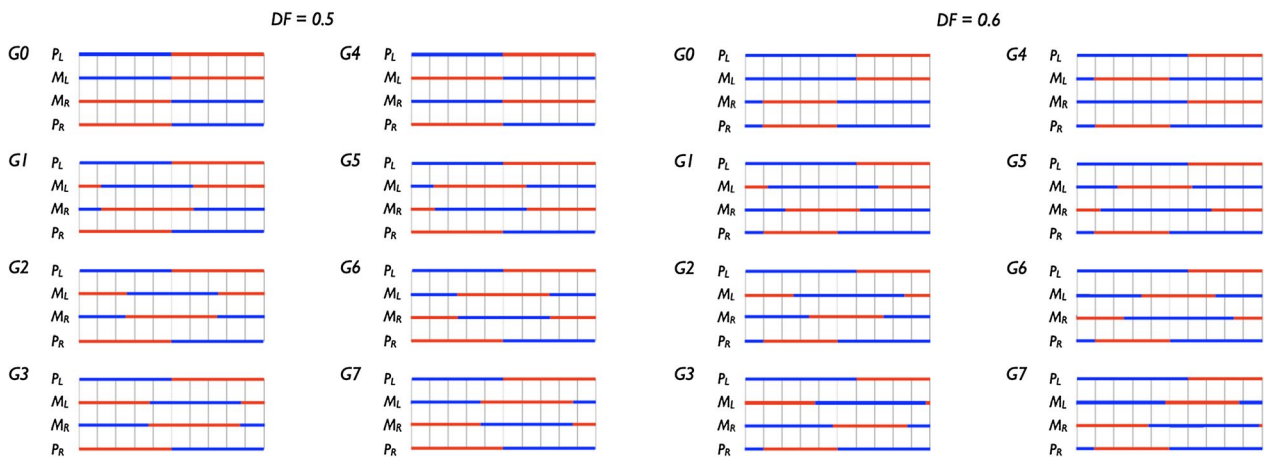

Fig. 2 The step cycles for gaits *G0*–*G7* are plotted for a duty factor $DF = 0.5$ (on left) and $DF = 0.6$ (right). Blue indicates the limb is in support, red indicates transition. For $DF = 0.6$ only *G0* and *G4* provide intervals with four limbs simultaneously in support

($LP = 0.25$), the latter having some of the dynamics of a run, with as few as one foot in support for short duty factors (Gambaryan, 1974; Hutchinson et al., 2003, 2006; Schmitt et al., 2006). Unfortunately, the term amble has also been used as a postulated sauropod gait (Casanovas et al., 1997; González Riga & Tomaselli, 2019; Vila et al, 2013), but their "amble pace gait" and "amble walking" are apparently synonymous with the *G0* pace.

We note that while given discrete names, behaving quadrupeds vary their limb phases by roughly ± 0.06 from stride to stride (Hildebrand, 1965, 1976, 1989). To explore possible sauropod trackmaker gaits, it is assumed that limb phase was at least 0.5, and therefore at least three limbs are in support during the step cycle. Hence we examine all combinations of eight discrete limb phases, three choices for overstepping (0, 1, 2), and three choices of duty factor ($DF = 0.5, 0.6, 0.75$). A given choice is reflected by the trial name, such as *G2-1-60*.

1.4 Track measurement uncertainty

The trackway data for the present study is from the massive, extraordinarily well-documented collection of Late Jurassic (Kimmeridgian) dinosaur ichnoassemblages near Porrentruy in the Canton Jura (NW Switzerland) (Marty, 2008; Marty et al., 2003, 2004, 2010; Paratte et al., 2018). During the excavation of Highway A16, over 14,000 tracks of both sauropod and tridactyl dinosaurs were discovered, distributed across 50 ichnoassemblages, and comprising about 230 tridactyl trackways and 260 sauropod trackways. Some paleosurfaces covered more than 4000 m^2 in area, the largest of which containing nearly uninterrupted trackways that extended for hundreds of meters.

Figure 3 shows an orthophotograph of the Courtedoux-Béchat Bovais tracksite (Early/Late Kimmeridgian Reuchenette Formation) of the Canton Jura, NW Switzerland (Marty et al., 2007). Note that some of the sauropod trackways show both manus and pes tracks while others are pes-only. Given that a manus track may either be missing or overprinted, this study selected only trackways containing both manus and pes tracks, to avoid that source of spatial uncertainty. Three trackway segments of the 500-level of this tracksite were selected, each approximately straight, with a regular pattern, and devoid of missing or overprinted tracks, and of sufficient length to analyze multiple complete step cycles: BEB-500-S1, BEB-500-S3, and BEB-500-S4, referred to here as S1, S3, and S4.

For the current study, a trackway is represented by the locations of its tracks. A physical track is a depression of the substrate that is often—but not invariably—surrounded by a raised displacement rim, and within which are sometimes preserved impressions of digital and metapodial pads and unguals Since the outline of a track is often difficult to distinguish from the surrounding substrate, and frequently is partly obliterated by another track, the preferred reference point marking the location of a track is the track 'center' (Leonardi, 1987; Lockley, 1991; Thulborn, 1990). A robust means to define the track center is provided by the following geometric construction (Marty, 2008). The sauropod tracks (both manus and pes) in this assemblage have displacement rims that are generally elliptical and approximately bilaterally symmetrical: a line segment can be constructed to represent the axis of symmetry which roughly bisects the track. A second line, perpendicular to the first, spans the track at its greatest width, and their intersection marks the track center. This geometric construction can be applied to both sauropod manus and pes tracks, especially those that are closed and isolated. Measurement uncertainty is greater for shallow tracks with an incompletely-closed displacement rim. The location of the center of each track was assigned an uncertainty from 1 cm (for tracks with the most symmetrical and sharply-defined displacement rims) to 5 cm (or more, in the case of the poorly-preserved tracks) to provide an estimation of the precision of each center; see measurement methods and track statistics in (Paratte et al., 2018; Stevens & Ernst, 2017).

While the dimensions of the displacement rim are greater than those of the trackmaker's foot, and its roughly elliptical shape is only a rough indicator of the foot morphology, the 'center' of the displacement rim permits a reasonably repeatable measurement of track location (Fig. 4). Pooling the 4207 sauropod pes tracks in the assemblages studied, the uncertainty-weighted median ratio $PL/PW = 1.3 \pm 0.13$, matching the ratio 1.31 measured for a well-preserved natural cast of a sauropod pes (Platt & Hasiotis, 2006), where the length included the claw marks. The median measurement uncertainty in PL and PW was about 2 cm. A track is therefore represented as a mathematical point with associated uncertainties ($x \pm dx$, $y \pm dy$) that reflect confidence in that location. Even a modest spatial uncertainty of a few percent, however, can become a significant limiting factor in the reliability of a computation due to error propagation.

2 Method

In a precursor to the current study (Stevens et al., 2016), a synthetic trackway generator showed that estimating gait (LP and DF) from a regular trackway pattern depends upon trackmaker size D_{GA} and yet trackmaker size cannot be sufficiently-precisely estimated from conventional track-based heuristics to disambiguate gait (see

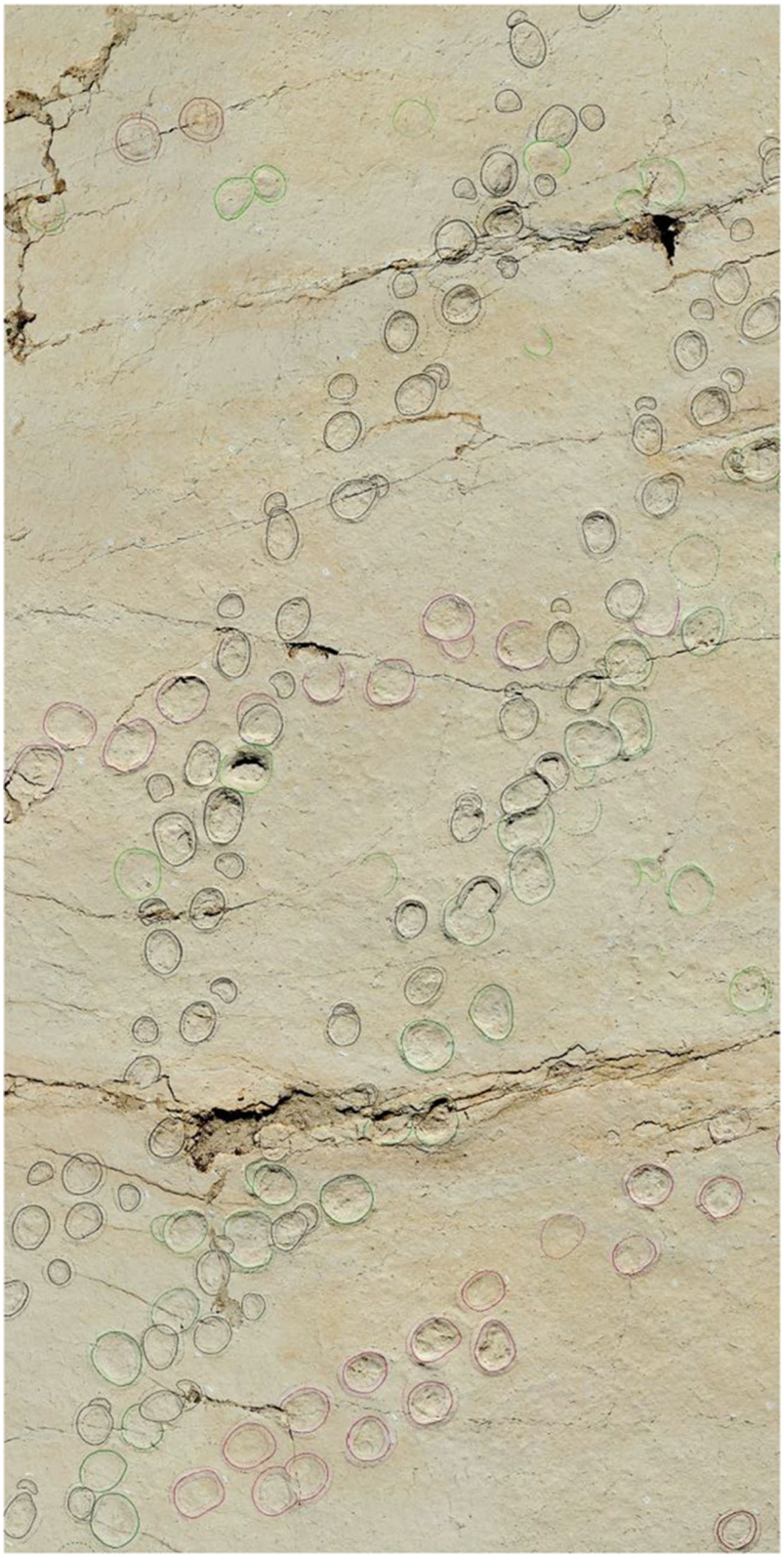

Fig. 3 An orthophotograph of a small portion of the BEB-515 level of the Courtedoux-Béchat Bovais tracksite. Note that multiple trackways were identified with differing trackway patterns (some have distinct manus and pes tracks, and others have only pes tracks). This image covers an area of 20 m by 10 m

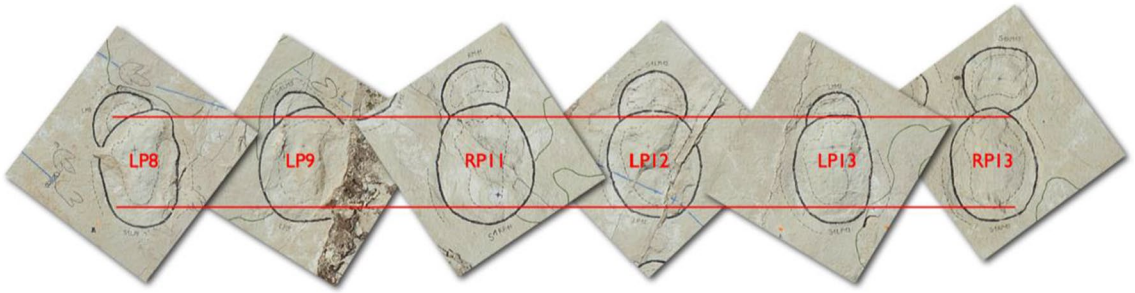

Fig. 4 Orthophotographs of well-preserved sauropod tracks from the BEB-500-S1 trackway of the Courtedoux-Béchat Bovais tracksite (Marty et al., 2007). The displacement rims (solid line) are roughly elliptical and the manus tracks are partly overprinted. Within the roughly elliptical displacement rim, the actual outline of the foot is often, but not invariably, apparent (outlined by dashed lines). The displacement rim is more reliably present and therefore used as the basis for locating track 'centers'. The red lines are separated by 50 cm

the Discussion section regarding the estimation of the uncertainty associated with those heuristics). It would appear a stalemate, for even if pes length were measured precisely, that precision would be overshadowed by the uncertainty in the proportionality constants used to estimate trackmaker size. Perhaps unintuitively, a source of trackway irregularity, which usually just adds statistical uncertainty to a trackway measurement (median stride length) might be used as a source of gait information to break this stalemate (Stevens et al., 2017).

Rather than consider a perfectly regular trackway, we examine a segment of an actual, hence slightly-irregular, trackway. An individual track (such as LP1 in Fig. 1) is represented by a mathematical point indicating its center, with an uncertainty associated with each coordinate. A trackway is represented by four ordered sequences of tracks (e.g., LP1, LP2, etc., for the left pes tracks in Fig. 1). The corresponding trackmaker is represented by the manus locators M_L and M_R and the pes locators P_L and P_R. Each locator is a mathematical point that represents the location of limb distal point of contact and which alternates between two states: support while that limb contributes to supporting the body, and transition as the limb takes the next step, according to a specified gait. When a locator is in support, its coordinates (and spatial uncertainty) correspond to that of the specific track it stands upon. When in transition, its coordinates are interpolated towards the next track, and assigned greater uncertainty during protraction. The trackmaker is simply a set of four independently moving locators, each given a specified sequence of tracks to step upon, and a prescribed timing and duration with which to do so.

A trial starts for a specified gait (*LP*, *DF*) at $t = 0.0$ with P_L having just stepped onto LP1; it remains stationary until $t = DF$, whereupon it proceeds towards LP2, arriving at $t = 1.0$ (one step cycle later). The left manus M_L can similarly be modeled according to those gait parameters, stepping from one manus track to the next according to its assigned track sequence. M_L begins support at $t = DF$ in the first cycle, and, depending upon the (unknown) degree of overstepping, it might initially step upon LM1, LM2, or even LM3 (Fig. 1). The trial *G2-1-60* would correspond to M_L upon LM2. These alternatives are examined in different trials rather than make any assumption about the degree of overstepping. For symmetrical gaits, the two hindlimbs are in counterphase, as are the two

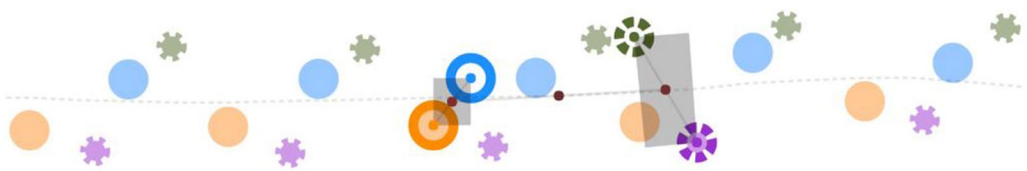

Fig. 5 A diagrammatic representation of a segment of a quadrupedal trackway as it is being traversed by a schematic trackmaker governed by a specific choice of gait parameters for this trial. The track locations are from the BEB-500 S1 trackway; the direction of travel was from left to right (closed shapes indicate the tracks, with pes tracks in blue and orange, and manus tracks in green and mauve). In this trial the gait is a walk ($LP = 0.25$, $DF = 0.5$). The trackmaker is indicated by the four locators (with open symbols, a blue ring for left pes, etc.). At the moment depicted, P_R, P_L, and M_R are in support and standing on tracks, and M_L is in transition. Line segments represent the manus and pes couplers, and the line segment *CL* that connected their midpoints represents the distance between the two couplers. The gray boxes represent the spatial uncertainty of each coupler

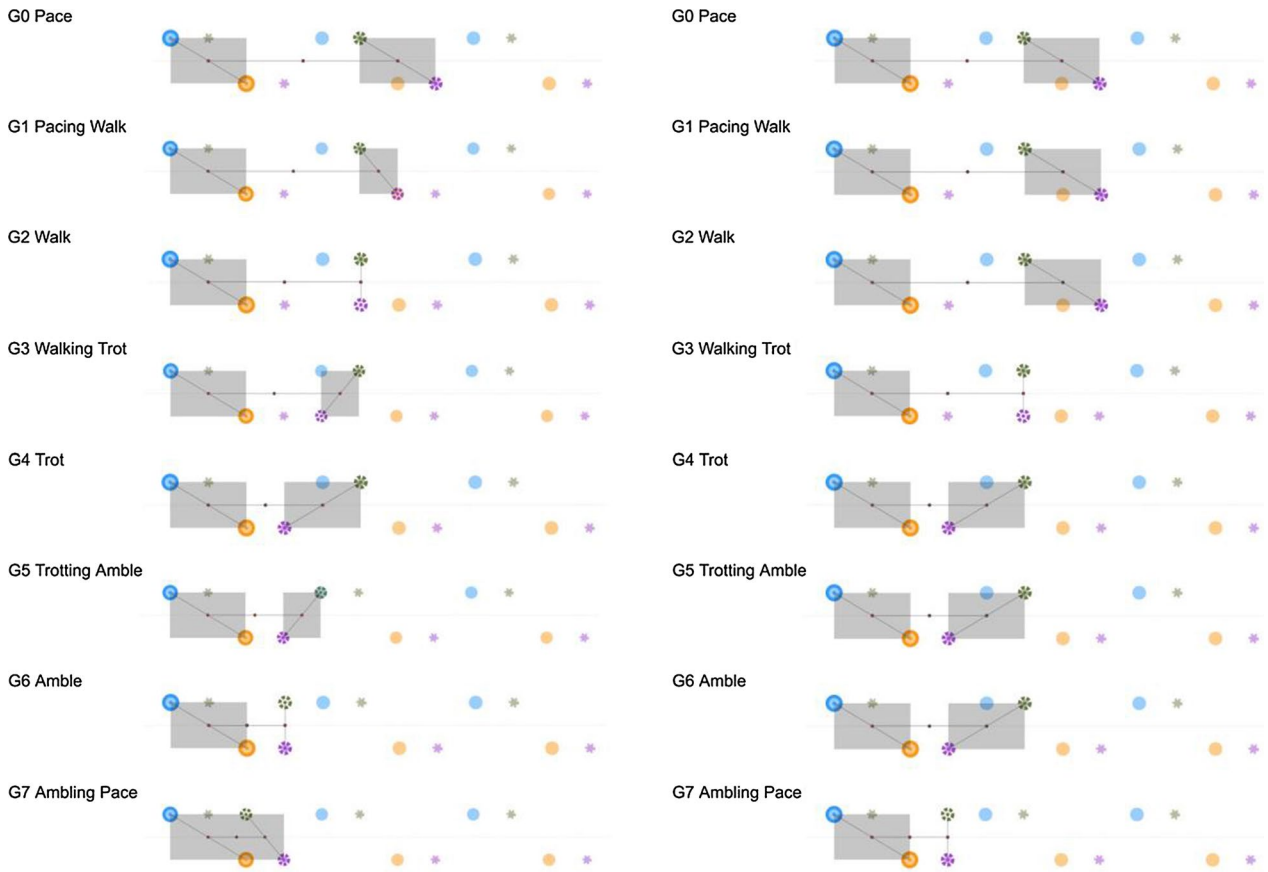

Fig. 6 Coupling length computations for the hypothetical regular trackway, for two choices of duty factor (*DF* = 0.5 on the left and 0.75 on the right) and the eight gaits (*G0–G7*). Each trial depicts the same point in a step cycle at which both hind limbs and the right forelimb are in support and the left pes is about to start transition. For the high duty factor trials (right column), note that *G0*, *G1*, and *G2* are consistent with the same *CL* (and likewise *G4*, *G5*, and *G6* would be consistent with a constant, but shorter, *CL*)

forelimbs, therefore P_R and M_R can be assigned their initial tracks and timing for $t = 0.0$.

This pairing between the two hindlimbs is represented by a pes coupler γ_{pes} (a line segment connecting P_L and P_R, the midpoint of which approximates the location of the acetabulum), and likewise a manus coupler γ_{manus} represents the coupling between M_L and M_R, and locates the pectoral girdle). The separation between locators γ_{pes} and γ_{manus} is termed the coupling length *CL* (Fig. 5) and is a generalization of the conventional computation of *GA* (Fig. 1). The derivation of CL is provided in Appendix 1 (see Eq. 4).

The position of each locator can be sampled at two moments within the step cycle: when it just reaches its next track, and when it just lifts from that track. During its interval of support, that locator has the spatial certainty of the track on which it stands. When that locator is in transition towards its next track its location is interpolated between its previous and next track with an uncertainty corresponding to the stride length (it could be anywhere between those tracks). Each coupler therefore alternates between having low spatial uncertainty when both locators are in support, and higher uncertainty otherwise. Coupling length, being the instantaneous distance between the two couplers, thus has variable uncertainty within each step cycle along a given trackway.

Even the most regular of trackways show subtle shifts in the placement of manus tracks relative to pes tracks—irregularities that reflect some unknown behavioral event such as a slight hesitation, change of speed, or reaction to the movements of other trackmakers. While the instantaneous separation between the girdles naturally varies during a step cycle (due to axial skeleton flexion, pectoral girdle mobility, etc.), it can be regarded as some (unknown) constant for the duration of the trackmaker's progression down a trackway. If a regular trackway shows a perturbation (e.g., shorter strides for a few cycles) that irregularity is attributed to a momentary change in gait, not a

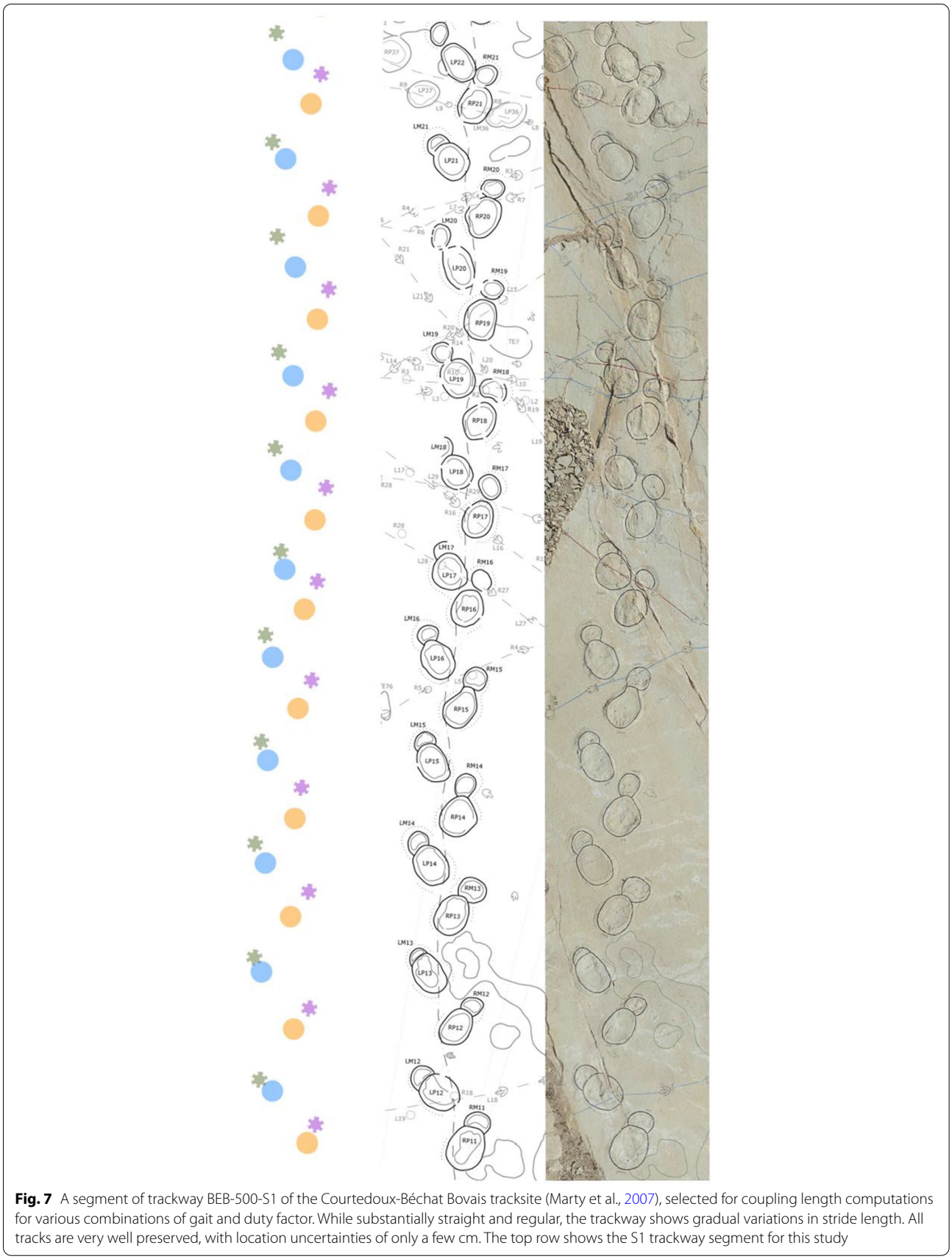

Fig. 7 A segment of trackway BEB-500-S1 of the Courtedoux-Béchat Bovais tracksite (Marty et al., 2007), selected for coupling length computations for various combinations of gait and duty factor. While substantially straight and regular, the trackway shows gradual variations in stride length. All tracks are very well preserved, with location uncertainties of only a few cm. The top row shows the S1 trackway segment for this study

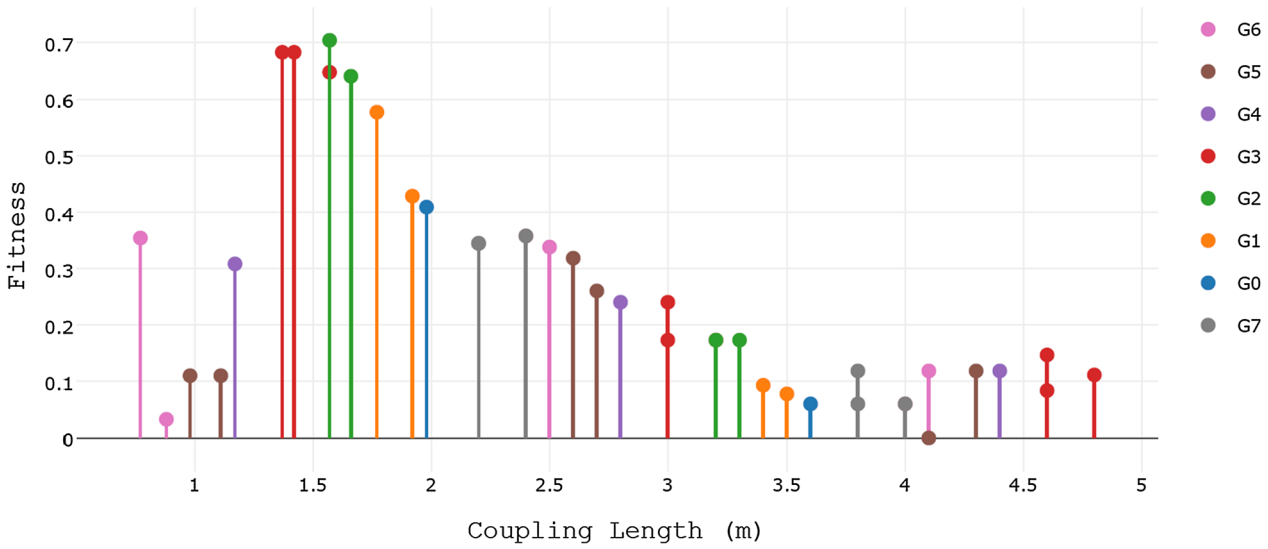

Fig. 8 Solution fitness

Table 2 Resultant coupling length values (with uncertainties) for the highest-fitness solutions for BEB-500 S1

Trial	Minimum CL (m)	Median CL (m)	Maximum CL (m)
G3-0-50	1.22 ± 0.08	1.37 ± 0.07	1.49 ± 0.08
G3-0-60	1.26 ± 0.08	1.42 ± 0.07	1.53 ± 0.08
G2-1-50	1.4 ± 0.08	1.57 ± 0.07	1.68 ± 0.08
G3-0-75	1.4 ± 0.08	1.57 ± 0.07	1.68 ± 0.08
G2-1-60	1.49 ± 0.08	1.67 ± 0.07	1.78 ± 0.08

The two closely-related gaits, the *G2-1* walk and the *G3-0* 'walking trot', have similar predictions for coupling length *CL* for a range of duty factors. The minimum and maximum values refer to the extremes of *CL* for each trial, straddling the median

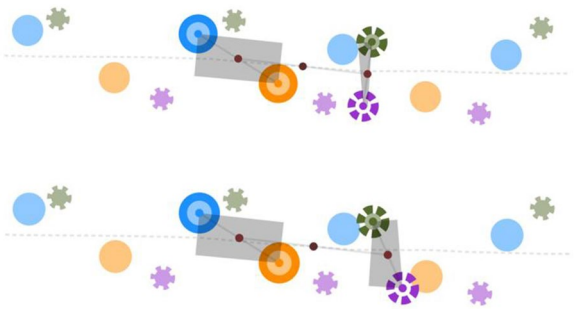

Fig. 9 The *G3-0–50* 'walking trot' (upper) and the *G2-1-50* walk (lower). Note the subtle difference in the position of the forelimbs and the roughly 20 cm difference in inferred trackmaker *CL*

change in gleno-acetabular length. If we then monitor the instantaneous coupling length for a trackmaker for a given hypothesized gait (e.g., *G2-1-60*), the trackway perturbation will be reflected in a corresponding perturbation in *CL*. Depending on the choice of gait, that variation might be "taken in stride" (with little variation in computed coupling length *CL*) or, for another choice of gait would require (in effect) a sudden acceleration or deceleration of one or more limbs to adjust the stride to accommodate the track positions in the vicinity of that irregularity, which is reflected in a sudden change in *CL*. By quantifying the magnitude of the perturbation in *CL*, we can compare the fitness of various hypothesized gaits for the given trackway.

The range of computed *CL* across the space of possible gaits is considerable, providing a basis for comparing alternatives despite the limitations posed by measurement uncertainty. Figure 6 illustrates alternative *CL* computations for an idealized trackway given different combinations of two duty factors ($DF = 0.50$, left column, and $DF = 0.75$, right column) and the eight gaits defined in Table 1.

The range of possible *CL* interpretations increases considerably when one then considers alternative pairs of manus tracks to associate with a given pair of pes tracks. For the lateral sequence gaits (*G0–G3*) in Fig. 6 the M_L is placed upon the second manus track ahead of the pes track on which P_L is standing. This is called 'tertiary overstep' (Peabody, 1959). We use a simple 'track separation' (of 0, 1, or 2) to indicate this choice of manus track, i.e., the number of manus tracks between P_L and M_L. For example, in the top row of Fig. 6, the gait is a *G0* pace, and the track separation is 1, so the gait is termed *G0-1*, to indicate one intervening manus track, as distinct from the (improbably) short-coupled *G0-0*, or the longer *G0-2*.

To explore the space of possible computations of *CL* for various hypothetical combinations of track separation, limb phase and duty factor, these variables were combined into a single experimental variable, α-phase. Coupling length *CL* could then be computed along a given real trackway, with two computations per step cycle, for any specific choice of α-phase.

A graph of *CL* along the trackway results in a curve that fluctuates about a median value. The median value corresponds to the gleno-acetabular distance for a trackmaker proceeding with that combination of limb phase and duty factor on that trackway. To compare *CL* across different hypothetical gaits for the same trackway, a fitness function was designed to quantify the local deviations of *CL* from the median value. The derivation of the fitness function is provided in Appendix 2 (see Eq. 20).

3 Results

Figure 7 shows the trackway segment S1 from track LP11 to track LP22. Given that coupling length can be measured twice per step cycle, we could gather 20 values of *CL* along this trackway segment. While at first glance S1 appears quite regular, note that stride length gradually decreases towards LP18 then increases from that point on.

The present method was first developed during the analysis of the S1 trackway, then it was applied to the S3 and S4 trackways. Coupling length *CL* was computed along the length of trackway S1 for each combination of the eight gaits (*G0*–*G7*), the three track separations (0, 1, or 2), and the three duty factors ($DF = 0.5$, 0.6, and 0.75). For example, for a *G4* trot, we examined all combinations of three track separations and three duty factors (*G4-0-50*, *G4-0-60*, *G4-0-75*, *G4-1-50*, etc.). We then excluded those combinations that would have placed the pes ahead of the manus at some point in the step cycle, resulting in a total of 40 trials.

The S1 trackway consists of 10 complete step cycles, sampled twice per cycle, resulting in 20 coupling length measurements per trial. We accumulated 40 such sets of *CL* measurements, and needed a way to compare them. We focussed upon the amount *CL* varied from cycle to cycle along the trackway in response to the slight irregularity in the trackway pattern. A fitness function was created to 'reward' or provide a better fitness score to trials in which *CL* showed less extreme relative fluctuation along the trackway (see Eq. 20, Appendix 2).

Figure 8 shows the resulting fitness functions values (ordinate) sorted by coupling length (abscissa). Note that the solution fitness is best in the vicinity of a coupling length of about 1.5 m, corresponding to a short-coupled *G3-0* walking trot (for three duty factors 0.5, 0.6, and 0.75) and a *G2-1* walk (for duty factors 0.5, and 0.6). These five trials were selected to consider in greater detail.

The five selected solutions pertain to only two close-related gaits: the *G2-1* walk and the short-coupled *G3-0* walking trot, which vary by only 0.125 in limb phase *LP* (from 0.25 to 0.375). The five solutions also represent a range of hypothesized duty factors from 0.5 to 0.75. As shown in Table 2, these combinations result in overlapping solutions that span only a narrow range of median *CL* from 1.37 to 1.67 ± 0.07 m, with a best fit length of 1.6 ± 0.2.

To appreciate the subtle differences in these solutions, Fig. 9 shows the placement of the four locators in the case of the *G3-0-50* walking trot versus the *G2-1-50* walk for the same duty factor ($DF = 0.5$). The solutions are diagrammed for the midpoint of the trackway segment, see Fig. 7), where a minimum in *CL* was observed (see Appendix 2, Fig. 17). The computation of *CL* along the trackway is shown in Fig. 10 for the five highest-fitness trials.

In addition to trackway S1, two additional trackways were analyzed: BEB-500-S3 and BEB-500-S4 of the same 500-level Courtedoux-Béchat Bovais tracksite. They are referred to here as the S3 and S4 trackways. The three trackways, S1, S3, and S4, had very similar track morphology and dimensions, but were following separate paths. S1 and S3 were slightly convergent straight paths about 20 m apart; S1 and S4 were straight, parallel, and separated by about 70 m.

The trackway pattern in S3 (Fig. 11), appears very similar to that of the S1 trackway (Fig. 7). The variation along the trackway is difficult to discern visually, but nonetheless, leads to a very distinctive signature in the fitness distribution (Fig. 11). As in the analysis of the S1 trackway, S3 revealed a cluster of high-fitness solutions around a coupling length of 1.6 ± 0.2. In fact, the distributions in Fig. 8 and Fig. 11 are statistically indistinguishable. The trackmakers appeared to have been of very similar size and engaged in basically the same gait.

Next, we analyzed the extraordinarily regular S4 segment (of BEB-500-S4 of the same 500-level Courtedoux-Béchat Bovais tracksite). Figure 12 shows the trackway pattern and the fitness results. Note the absence of a cluster of high-fitness solutions. The S4 segment was apparently too regular, and any 'signal' to indicate the trackmaker's gait was masked by measurement uncertainty. The gradual increase in fitness with *CL* reflects a residual scaling effect (see Appendix 2).

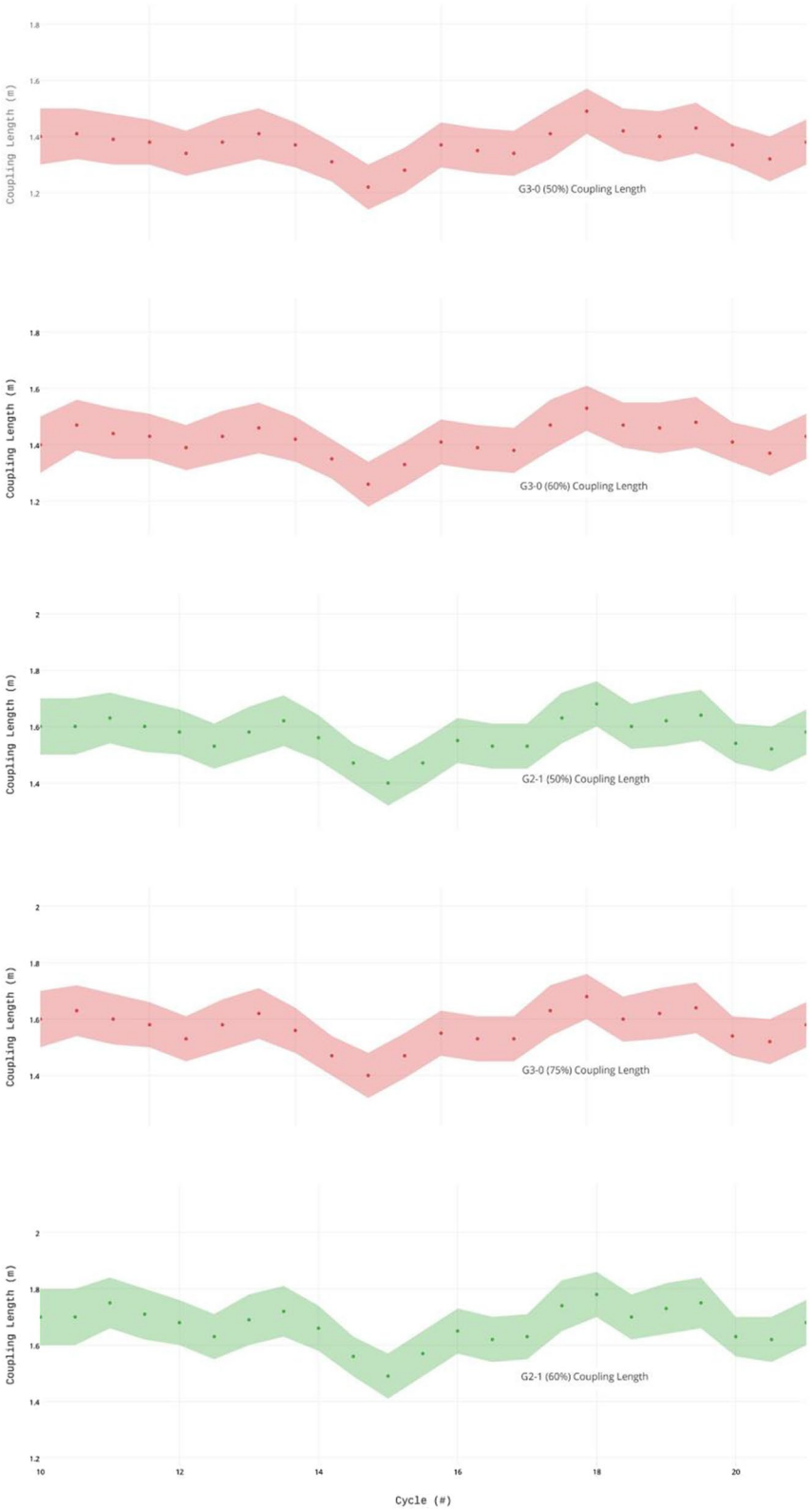

Fig. 10 Coupling length computations for the five trials showing the best solution fitness (Table 2). These correspond to a small range of gaits (*G2* walk and *G3* walking trot) and duty factors

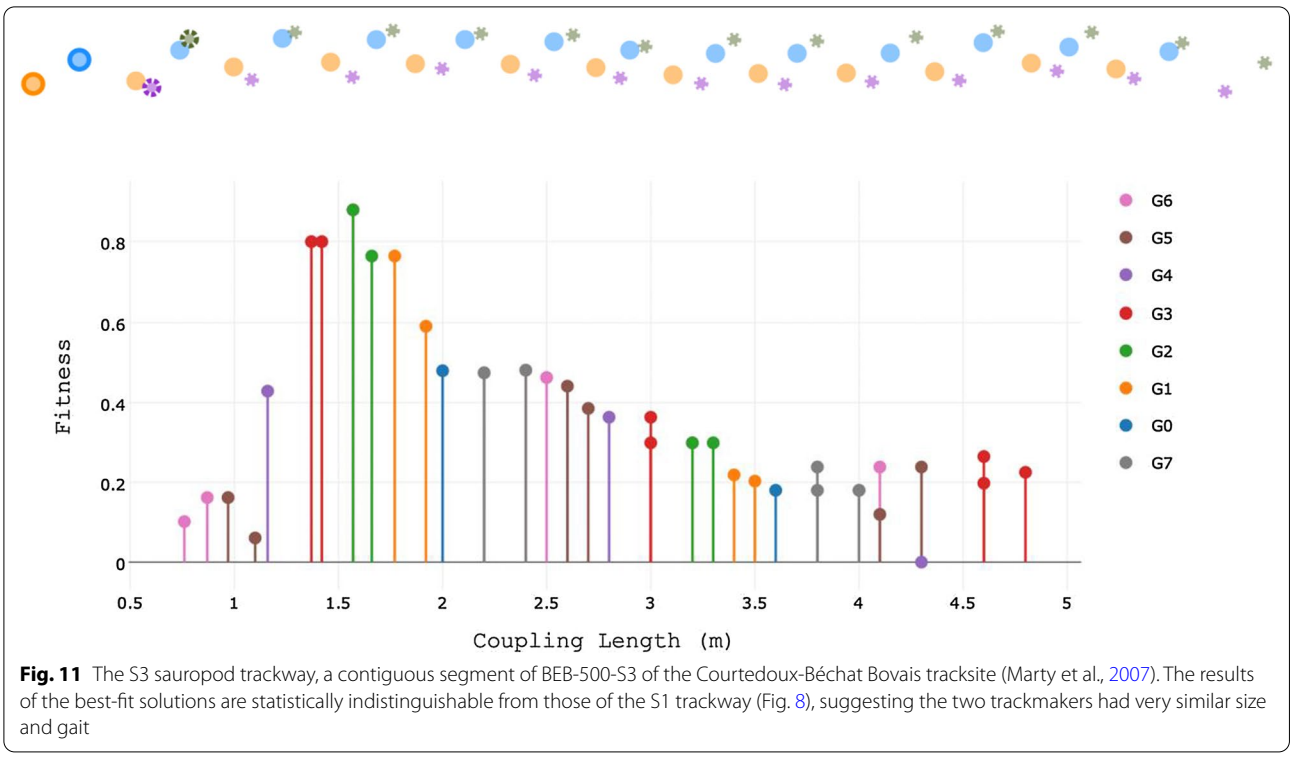

Fig. 11 The S3 sauropod trackway, a contiguous segment of BEB-500-S3 of the Courtedoux-Béchat Bovais tracksite (Marty et al., 2007). The results of the best-fit solutions are statistically indistinguishable from those of the S1 trackway (Fig. 8), suggesting the two trackmakers had very similar size and gait

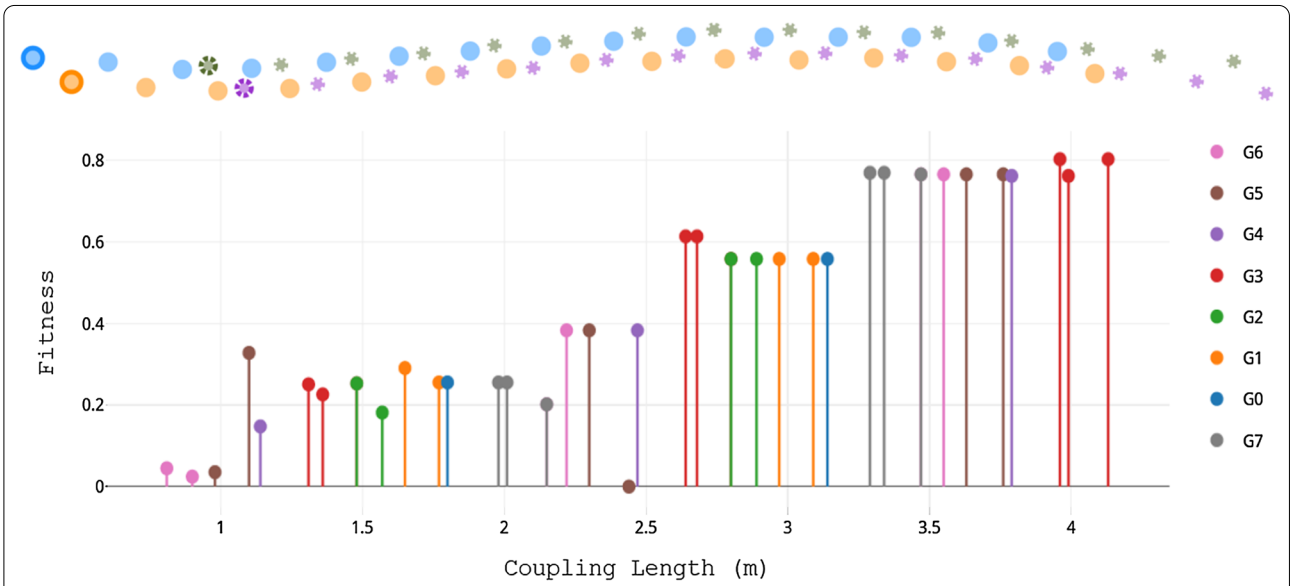

Fig. 12 The S4 trackway, a contiguous segment of BEB-500-S4, presented insufficient irregularity to provide information about the gait or size of the trackmaker based on coupling length

4 Discussion

4.1 High-fitness solutions

Evaluating the fitness function across the combinations of gait and duty factor applied to BEB-500 S1 and S3, it was found that those combinations corresponding to a median gleno-acetabular distance of about 1.5 m show markedly less persistent deviation from the median (hence they represent better solutions) than those that produced by either shorter or longer-coupled trackmakers. In other words, if the trackmaker had a D_{GA}

of about 1.5 m and proceeded with a gait with limb phase between 0.25 and 0.375 (i.e., a *G2* or *G3* gait) with relatively relaxed duty factors of between 0.5 and 0.75, that it could have created the variations along the trackway in S1 or S3 with the least variation in its gait. The fitness function showed which combinations of gait parameters resulted in the least variation in apparent axial length from hip to shoulder. Stated another way, presuming that the trackmaker maintained a constant body length, if it were to have walked with any other gait, it would have had to shift those gait parameters much more while only producing the subtle variation we observe along the S1 or S3 trackway. The failure to detect a high fitness solution for S4 demonstrates that the method is not robust. This method, without further constraints applied, only admits a resolution of *CL* under 'Goldilocks' conditions (i.e., trackways that are regular, but not too regular, relative to the spatial uncertainty created by measurement error).

For both S1 and S3 the best fit solutions were closely clustered, with three *G3-0* trials (with $DF = 0.5$, 0.6, and 0.75), and two *G2-1* trials (for $DF = 0.5$ and 0.6). Bearing in mind that the approach is probabilistic, these alternative solutions correspond to nearly the same footfall pattern and imply a trackmaker of nearly the same length for each best fit solution (Fig. 9). This analysis cannot resolve limb phase more precisely than to bracket it between a lateral-sequence singlefoot (walk) and a lateral-sequence diagonal-sequence gait (a 'walking trot' as it has characteristics of both a walk and a trot). The high-fitness S1 and S3 solutions have an honorable mention: the *G1-1-50* ('walking pace'), which corresponded to a slightly longer D_{GA} of about 1.8 m. It is noteworthy that all the high-fitness solutions are in the range of *G1*–*G3*. Given the limited precision by which limb phase can be resolved using this method, it is helpful to consider what the analysis *rules out*, namely the *G4* trot and any other *diagonal-sequence* gait (*G4*–*G7*). It also indirectly rules out any solutions for trackmaker length other than those within a narrow band of D_{GA}. There was also no support for the suggestion that sauropods engaged in a *G0* pace, contra (Casanovas et al., 1997; González Riga & Tomaselli, 2019; Vila et al., 2013).

Diagonal couplet gaits (*G3* through *G5*) are regarded as primitive for tetrapods, while lateral couplet gaits (*G1* through *G2*) may be a "true mammalian innovation" (Wimberly et al., 2021). Sauropods, on that basis, might have been expected to have used a *G4* trot, but the elephant, being the largest extant terrestrial vertebrate, has been a more frequent model for sauropod locomotion, and so sauropods are usually depicted with a lumbering walk. Elephants always use lateral sequence gaits that vary continuously from a lateral couplet (*G1* with *LP* about 0.2) at slower speeds to a singlefoot walk (*G2* with $LP = 0.25$) (Genin et al., 2010; Hutchinson et al., 2006). The result of our analysis suggests the sauropod trackmakers for the S1 and S3 trackways were engaged in lateral sequence gaits. Specifically, the set of highest likelihood solutions consisted of one *G1*, two *G2*, and three *G3* gaits. Duty factor in some solutions was a brisk 0.5, and in one solution, a sauntering 0.75.

Gait naming conventions tend to suggest sharp categorical distinctions (e.g., between lateral couplet and singlefoot, or between singlefoot and diagonal couplet), slight variations in limb phase in the vicinity of a walk produce very similar trackway patterns, and very similar footfall patterns in the trackmaker. Whether a sauropod was engaged in a "true" *G2* singlefoot or a *G3* diagonal couplet cannot be resolved by our analysis, unfortunately. What can be offered, however, is that the high-fitness solution set includes several potential gaits that are regarded as more mammalian than archosaurian.

4.2 Estimation of trackmaker size

Track-based estimation of body size proceeds in two heuristic steps. First, hip height H_A is estimated by multiplying measured pes track length *PL* by an assumed proportionality constant H_A/PL. Secondly, body length D_{GA} is estimated by multiplying the hip height estimate by another presumed linear proportionality D_{GA}/H_A:

$$D_{GA} = \frac{H_A}{PL} \times \frac{D_{GA}}{H_A} \times PL \tag{1}$$

Each term has associated uncertainty. Proposals for the first constant, H_A/PL, range from as low as 2.8 (Tschopp et al., 2015) to as high as 5.9 (Thulborn, 1990), with most estimates around 4 (Alexander, 1976; González Riga, 2011; Ishigaki, 1988; Vila et al., 2013). This large range reflects uncertainty in the contribution of soft tissues, the degree of digidigrady in the pes, and taxonomic and ontogenetic variations (e.g., Gallup, 1989; Bonnan, 2005; Wilhite, 2005; Schwarz, Wings, et al., 2007a; Schwarz, Ikejiri, et al., 2007b; Bonnan et al., 2010; Holliday et al., 2010; González Riga, 2011). Since neither the taxonomy nor the maturity of the trackmakers responsible for the trackways in this study is known, the heuristic H_A/PL is roughly 3.3 ± 0.5 (i.e., an uncertainty of about 15%).

The second proportionality constant, D_{GA}/H_A, also varies considerably across sauropod taxa, ontogeny, and the skeletal reconstruction. Proposals for this constant based on earlier skeletal reconstructions vary from 0.92 to 1.2 (González Riga, 2011; González Riga & Tomaselli, 2019; Mazzetta & Blanco, 2001; Vila et al., 2013), but those reconstructions have evolved over the last century, with

more recent reconstructions corresponding to D_{GA}/H_A of 1.0 or less, especially in subadults and juveniles due to their relatively longer limbs (Lovelace et al., 2007; Schwarz, Ikejiri, et al., 2007b; Stevens, 2013; Stevens et al., 2016; Woodruff & Foster, 2017; Woodruff et al., 2018). Here we assume $D_{GA}/H_A = 1.0 \pm 0.1$. Given that the median pes track length PL along the S1 trackway was 0.48 ± 0.08 m (i.e., an uncertainty of about 17%), the estimate for trackmaker size, incorporating error propagation in Eq. 1 is:

$$D_{GA} = \frac{H_A}{PL} \times \frac{D_{GA}}{H_A} \times PL = 3.3 \times 1.0 \times 0.48 = 1.6 \pm 0.4 \text{ m} \quad (\text{i.e., } \sim 25\% \text{ uncertainty}) \qquad (2)$$

Of course, the uncertainty would be less for a known trackmaker of known maturity, but for the sauropod trackways such as those in the assemblages studied here both those factors are unknown. The best fit trackmaker length D_{GA} based on coupling length was 1.6 ± 0.2 m. Given the very different sources of information on which the two measurements are based, it is noteworthy that the estimates are so similar. The estimate of D_{GA} based on coupling length is thus about twice as precise.

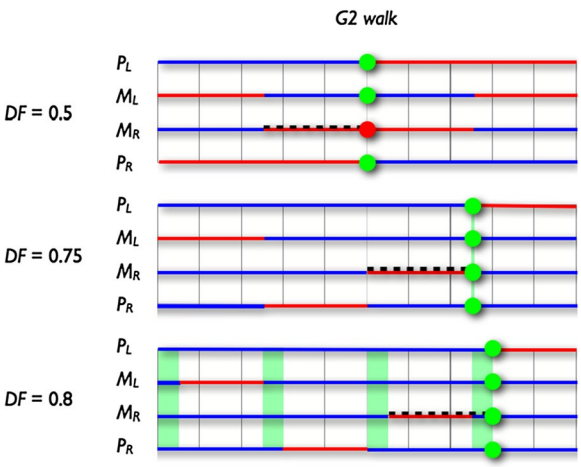

Fig. 13 The step cycle for a *G2* walk for three different duty factors (*DF*), with blue indicating support and red indicating transition states. We consider the case when P_L finishes support, and examine the state of the other three locators. For $DF = 0.5$ (top graph), at that moment, indicated by the colored dots, we see that only three of the four locators are in ground contact (green), while M_R is in transition (red) and its location must be interpolated. For $DF \geq 0.75$ (lower two graphs) M_R has completed its step and all four limbs are in ground contact. The dashed black line indicates the relative phase between M_R and P_L

5 Conclusions

It is computationally difficult to rigorously infer the size and gait pattern of a trackmaker from a trackway pattern. The extraordinary preservation of the tracks on the BEB-500 level provided numerous trackway segments that were promising but for the absence of a manus print or two. Perhaps those tracks were overprinted, or perhaps they were simply not preserved. Given the positional uncertainty with which even the best-preserved tracks could be located, we were limited to only those trackway segments that were complete in providing every manus and pes track along a contiguous length of the trackway. Of those, we were further limited to only those segments where the trackway indicated by its regularity a constant forward progression of steps, i.e., a constant gait. Two of these, trackways S1 and S3, were indeed useful and yielded results, but the especially regular trackway S4 reminded us that a regular trackway is fundamentally ambiguous (Stevens et al., 2016), i.e., any repeating pattern of tracks could have been produced by some corresponding combination of trackmaker size and gait parameters.

Our probabilistic approach incorporated the conventional numerical method of explicit error propagation, which allowed quantifying the confidence with which a signal could be resolved distinctly from the noise. It struck us as noteworthy that trackway irregularity, usually a source of obfuscation when attempting to derive insights by statistics, actually carries a useful signal to be interpreted. The strategy described here was the first use of track irregularities to resolve gait ambiguity and permit trackmaker size estimation. It was originally presented in 2017 (Stevens et al., 2017), and the coupling length method was described in the final report summarizing our work with the work on the sauropod trackway assemblages in the Canton Jura (Paratte et al., 2018; Stevens & Ernst, 2017). We concluded at the time that the sauropod trackmakers were engaged in a lateral sequence gait with limb phase corresponding to somewhere between a singlefoot (*G2* walk) and a diagonal couplet (*G3*), and as the method was founded upon a careful use of explicit error estimation, the estimate of D_{GA} provided by our method is consistent with, but offers greater precision than, the track-based methods which rely on heuristic coefficients of proportionality. The small absolute size of these sauropods, with a D_{GA} of roughly 1.6 m, was somewhat contrary to the usual expectation for gigantism in sauropods.

The present method was developed to provide some traction to the estimation of trackmaker size and gait in the case of extinct, graviportal, quadrupedal dinosaurs. Being graviportal, we assume these trackmakers were not engaging in running gaits, but that they used a symmetrical gait. Instead of assuming a specific gait (as a requisite for estimating trackmaker size from *GA*), the coupling length computation represents a

trackway-based measurement that generalizes over gait. The variation in *CL* along a trackway provides a means to explore the goodness of fit of various hypothetical choices of trackmaker gait. Our method also provides independent support for recent suggestions that H_A/PL is less than often proposed, and perhaps about 3.3 ± 0.7.

Clearly, there is much more to be done to study the robustness of this method. It is fragile, and it has not yet been tested against the trackways created by extant quadrupeds, for which both gait and size are known. On the other hand, this method attempts to infer the most that can be derived with the least assumptions one may make, namely that trackmaker had a relatively fixed body length and was engaged in a specific gait that could take in stride the slight variations observed in those trackways.

We emphasize again that the method does not model any kinematic chain (e.g., from manus locator to manus coupler to pes coupler to pes locator). This was intentional, for one can always create an increasingly specific model provided one wishes to introduce increasingly specific assumptions (for example, that the trackmaker was of one or another specific sauropod taxon).

Appendix 1

Coupling length

The interpretation of coupling length starts with selecting four tracks, two pes and two corresponding manus tracks. Since alternative pairs of manus tracks could have been selected to pair with the given pes tracks, the subsequent analysis begins with one such choice of pairings, which will then be generalized to explore other possible pairings of manus and pes tracks.

Next, we construct two couplers, one for the pair of pes locators and another for the pair of manus locators. In general, a coupler is a line segment representing the pairing of two locators (x_l, y_l) and (x_r, y_r), and its midpoint γ is simply given by:

$$\gamma = \left(\frac{x_l + x_r}{2}, \frac{y_l + y_r}{2} \right) \tag{3}$$

The midpoint γ of a coupler approximates the center of a limb girdle, therefore the coupling length *CL* is the instantaneous separation between the pes and manus couplers, specifically:

$$CL = \sqrt{\left(x_{\gamma,pes} - x_{\gamma,manus}\right)^2 + \left(y_{\gamma,pes} - y_{\gamma,manus}\right)^2} \tag{4}$$

where $x_{\gamma,pes}$ corresponds to the x coordinate of the pes coupler, and so forth. Figure 5 shows the pes and manus couplers as line segments between corresponding pes and manus locators, and the line segment *CL* is shown connecting the midpoints of the two couplers.

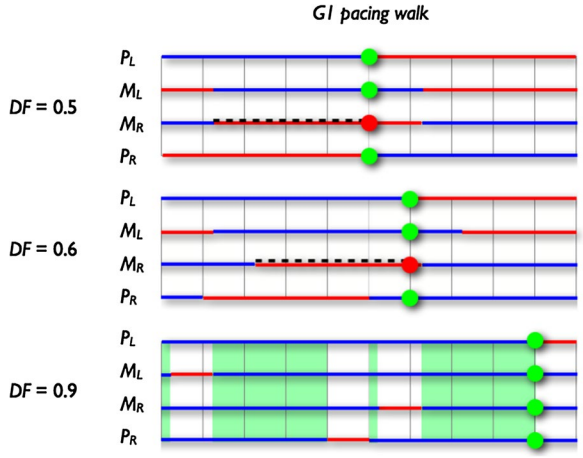

Fig. 15 The step cycle for a *G1* 'pacing walk' for three different duty factors (*DF*). For $DF = 0.5$ and 0.6 the right manus is in transition and must have its position interpolated. For $DF \geq 0.625$ all four limbs are in ground contact. As in Fig. 13, the dashed black line indicates α-phase ϕ_α the relative phase between M_R and P_L

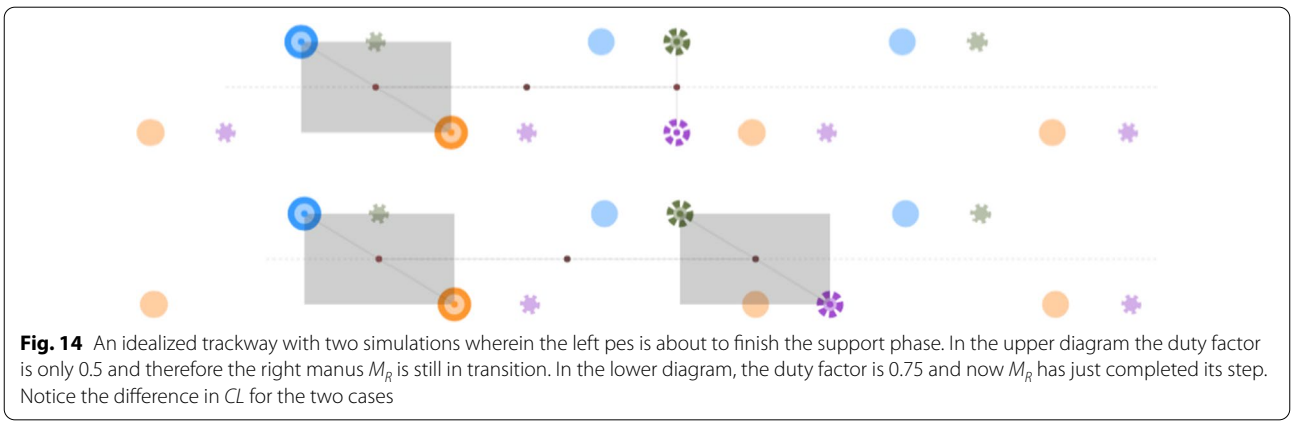

Fig. 14 An idealized trackway with two simulations wherein the left pes is about to finish the support phase. In the upper diagram the duty factor is only 0.5 and therefore the right manus M_R is still in transition. In the lower diagram, the duty factor is 0.75 and now M_R has just completed its step. Notice the difference in *CL* for the two cases

Table 3 The α-phase φ_α and the minimum duty factor DF_{Min} required to achieve four-limb support for each given gait

Gait		φ_α	DF_{Min}
Pace	*G0*	0	0
'Pacing walk'	*G1*	0.375	0.625
Walk	*G2*	0.25	0.75
'Walking trot'	*G3*	0.125	0.875
Trot	*G4*	0	0
'Trotting amble'	*G5*	0.375	0.625
Amble	*G6*	0.25	0.75
'Ambling pace'	*G7*	0.125	0.875

Coupling length is subject to measurement uncertainty since it is a computation based on uncertain locator positions. The positional uncertainty of a locator reflects the underlying track measurement error when in support, and that uncertainty is necessarily greater when the limb is stepping between tracks. When the locator is in midstep, its position is calculated using linear interpolation between the coordinates of the previous and next track centers, using a conventional interpolation variable α ($0 \le \alpha \le 1$). Initially (at $\alpha = 0$), the locator is still at the previous track, and is just finishing support. For intermediate values of α ($0 < \alpha < 1$) the locator is in transition and its position is interpolated between that of the previous and next tracks. When α reaches 1 the locator is again in support at the next track. Note that α is a relative phase, i.e., relative to when the locator begins transition, which depends on *LP* and *DF* and the particular limb. We will need to also compute the absolute phase (i.e., relative to P_L) at which to start the interpolation for that locator, which is specific to the limb, the limb phase, and the duty factor. Given that, we can then compute the position of each of the four limbs even if one limb is in transition, at any point within the overall step cycle.

Since we consider only walking gaits ($DF > 0.5$), both hindlimbs are simultaneously in support during two intervals of each step cycle. We measure *CL* only at the end of each such interval (when either pes P_L or P_R just finishes its support phase and begins its next step). This choice of timing will be shown to permit *CL* to converge to *GL*. At those two moments within a cycle, we know the position of the pes coupler γ_{pes} since both pes locators are in support, placed on their respective tracks. In the following, we describe only the case for P_L since the reasoning is similar for P_R. Since $DF > 0.5$ we also know that one manus locator is also in support, hence we know the position of the track on which it stands, and finally, we can also interpolate the position of the other manus locator. With both manus locators known, we can then solve for the position γ_M of the manus coupler and thus compute $CL = (\gamma_{manus} - \gamma_{pes})$ according to Eq. 4 for any combination of limb phase and duty factor $DF \ge 0.5$.

Coupling length for the walk gait

The equation for coupling length will be developed first for the familiar case of a *G2* walk ($LP = 0.25$), then will be generalized to other gaits. Figure 13 shows phase diagrams for the walk for three duty factors ($DF = 0.5$, 0.75, and 0.8). As in Fig. 2, the blue and red intervals indicate support and transition, respectively. In each case, a step cycle begins with the left pes P_L just beginning support, followed by the left manus M_L

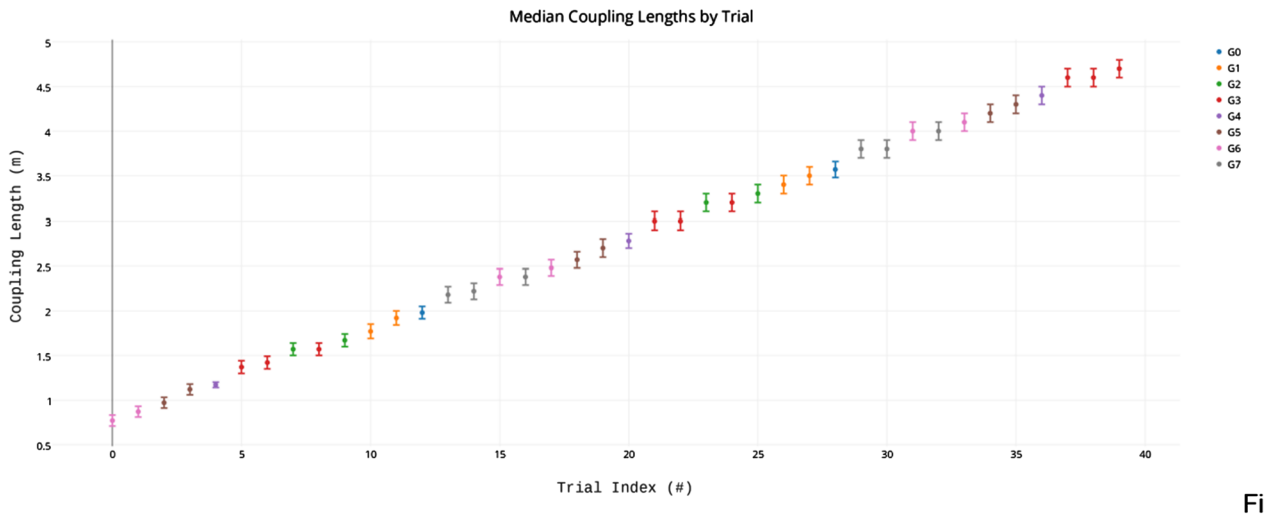

Fig. 16 Median Coupling lengths by trial. Note the color code indicating gait (*G0–G7*)

at $t=0.25$, the right pes P_R at 0.5, and the right manus M_R at $t=0.75$.

Coupling length is defined twice per step cycle (when either the left or right pes completes support and begins transition), but for purposes of development we consider when the left pes P_L just finishes support and begins to step. The state of the four locators is examined at this instant for three examples of duty factor (Fig. 13). For the very short duty factor of 0.5, note that while three locators are in support (indicated by green dots), M_R is in transition (red dot), midway between the previous and next track at that instant. Note that for longer duty factors (wherein P_L remains in support longer), M_R will complete more of its transition and converge on the location of the next track at that moment of measurement. For sufficiently long duty factors (i.e., $DF \geq 0.75$), all four locators are in support at that moment.

The left pes P_L begins support at time $t=0.0$ and it remains in support until $t=DF$ whereupon it begins transition. At that moment, the right manus M_R is still in transition for any duty factor less than 0.75, and its position would have to be interpolated as a fraction α of the distance between the last position for M_R and its next position. For the case of a *G2* walk ($LP=0.25$), the interpolation value α_{walk} depends only on the duty factor *DF*, and is given by:

$$\alpha_{walk} = \frac{0.25}{1.0 - DF} \tag{5}$$

The numerator of (5) is the relative phase between M_R and P_L, indicated by the dashed black line in Fig. 13 highlighting the fraction of a step cycle between the end of support for P_L and the end of support for M_R. The denominator of (5) is the duration in which the limb is in transition (i.e., it is the relative complement of the duty factor). The quotient α_{walk} is therefore the fraction of the way that

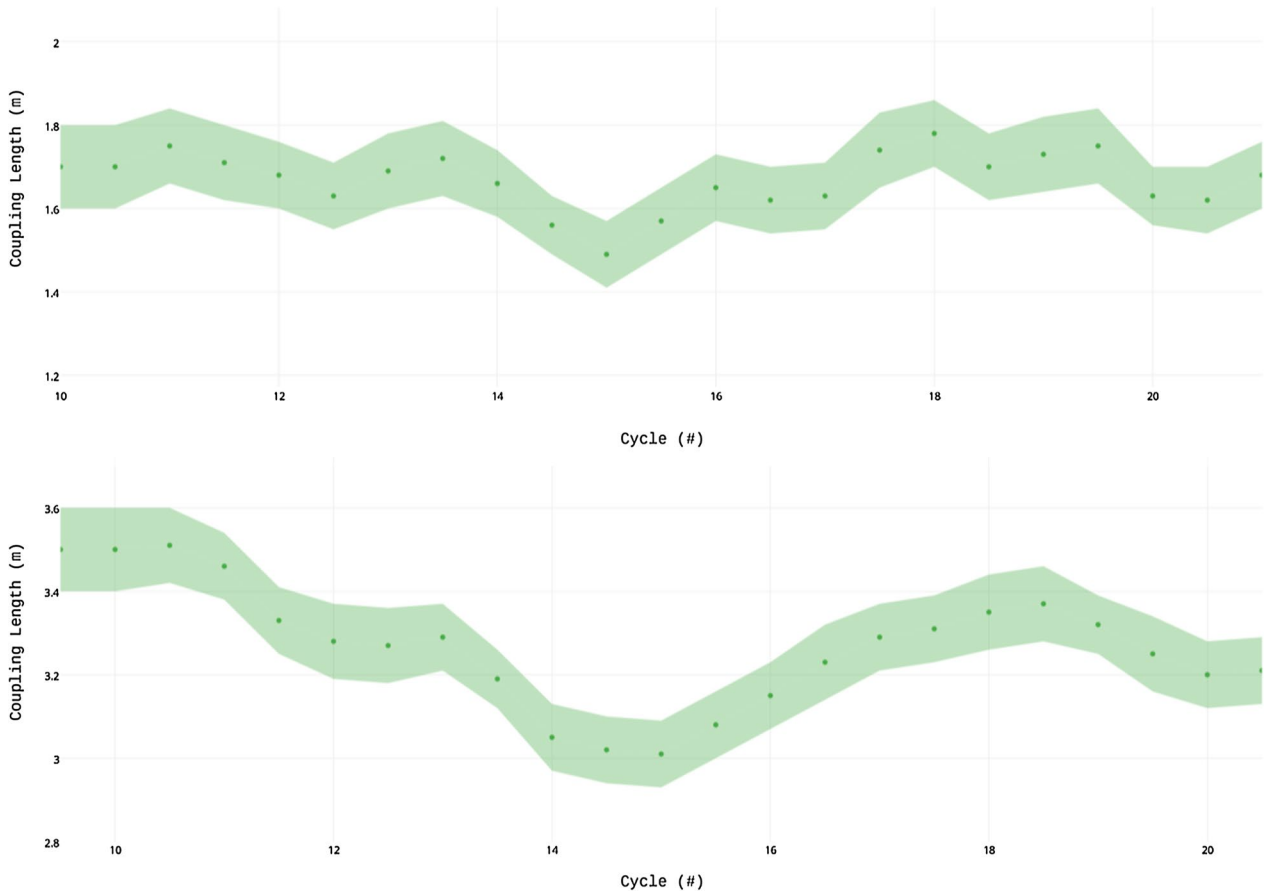

Fig. 17 Two trials for which coupling length is computed along the BEB-500-S1 trackway for a *G2* walk ($LP=0.25$, $DF=0.6$). Upper: shows the *G2-1-60* gait with track separation of 1 (refer to Fig. 6 for the track configuration corresponding to *G2-1)*. Lower: the same trackway and gait but for *G2-2-60* (i.e., a track separation of 2)

M_R has traveled from the previous track to the next track. For $DF = 0.5$, M_R is half the distance between the previous and next tracks, and for any value $DF \geq 0.75$ the interpolation would be complete, and M_R would be at the next track. What are the consequences of interpolation on the coupling length computation CL? Since P_L and P_R are in support, the pes coupler γ_{pes} is fixed, and M_L is also in support at this moment, so that as M_R converges on the next track as DF increases, CL converges on GA.

Figure 14 shows this diagrammatically for $DF = 0.5$ (upper trackway diagram) and $DF = 0.75$ (lower). The gait in both cases is a $G2$ walk ($LP = 0.25$). Both diagrams show the configuration of the four locators at the instant the left hindlimb is about to initiate another step. For $DF = 0.5$ the right manus is in transition midway between two manus tracks while for $DF = 0.75$ its transition phase is complete, all locators correspond to track positions, and CL converges to the conventional GL computation (Fig. 1). For values of $DF > 0.75$, CL would remain as shown in the lower diagram of Fig. 14.

Generalization to other gaits

The above discussion, while specific to the $G2$ walk, also applies to the other lateral sequence gaits such as $G1$ and $G3$. Recall that in the case of the walk, depending upon the duty factor, the right manus might still be in transition when we need to compute the location of the manus coupler. We interpolate the position of M_R between the previous and next right manus tracks using an interpolation value α_{walk}. While this interpolation value depended only upon the duty factor in Eq. 5. The generalization of (5) to apply to other gaits will depend on both LP and DF.

To illustrate, Fig. 15 diagrams the $G1$ gait (lateral sequence lateral couplet, $LP = 0.125$), for three duty factors ($DF = 0.5$, 0.6, and 0.9). Recall that the numerator in (5) was graphically indicated by the dashed black line in Fig. 13. The generalization of the numerator, which will be called the α-phase and given the variable ϕ_α below (in Table 3 and Eq. 6), is graphically indicated by the dashed black line in Fig. 15.

The generalization of the interpolation value α is now an equation with two unknowns, the α-phase ϕ_α (which is itself a function of LP and DF), and the duty factor DF:

$$\alpha(\phi_\alpha, DF) = f(x) = \begin{cases} 1; & if\ \phi_\alpha \geq 1.0 - DF \\ \frac{\phi_\alpha}{1.0 - DF} & otherwise \end{cases} \tag{6}$$

Table 3 shows the values of α-phase and the minimum duty factor DF_{Min} required to achieve four-limb support, for each of the eight gaits considered. This generalization extends to diagonal sequence gaits $G5$-$G7$, wherein the three-limb support is provided by P_L, P_R, and M_R and M_L in transition (and the α-phase is then measured between M_L and the pes P_L).

Coupling length CL can now be measured as the distance between the pes and manus couplers for any walking gait. In each case, the two pes locators are in support and one or the other manus locator may require linear interpolation, by:

$$\gamma_{manus} = \left(\frac{x_1 + x_{2,prev} + \alpha\left(x_{2,next} - x_{2,prev}\right)}{2}, \frac{y_1 + y_{2,prev} + \alpha\left(y_{2,next} - y_{2,prev}\right)}{2} \right) \tag{7}$$

where $\psi 1$ is the locator in support, $(x_{\psi 1}, y_{\psi 1})$ is the position of that locator, and $\psi 2$ refers to the other locator which is in transition, the position of which is being interpolated.

This formula reduces to the original GA formula when α is 0 or 1, i.e., when the duty factor is sufficiently long to permit all four limbs to be in simultaneous ground contact for that given gait. Coupling length is therefore a discretely sampled, periodic value within a trackway that can be measured twice per gait cycle (each time a pes support cycle ends).

Given that the S1 trackway consists of 10 complete step cycles, each trial resulted in 20 coupling length measurements (twice per cycle for 10 cycles). Median CL was then computed for each trial for the 20 coupling lengths. Figure 16 plots the results sorted by median CL length. No coupling lengths were excluded, resulting in some improbably short-coupled ($CL = 0.77$ m) and some

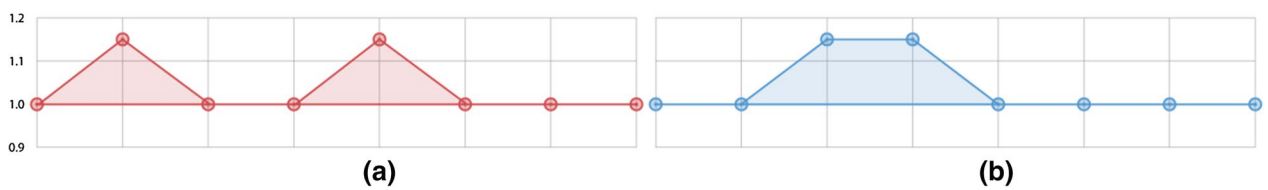

Fig. 18 In *a*, coupling length increases from a median value at two separate points along the trackway, while in *b*, this shift occurs once, but for a longer duration. Note that the area under the two curves is identical

improbably long-coupled ($CL = 4.7$ m) trackmakers for the size of the tracks in this trackway. Each computed value of *CL* also has an associated uncertainty which reflects error propagation from the uncertainty in the track locations. Despite the excellent preservation of this trackway, the small uncertainties in track position result in a large degree of overlap between median coupling length values in neighboring solutions. While trials with shorter *CL* have a greater relative uncertainty than those with longer values of *CL*, the median values by themselves provide very little information. Not finding any distinguishing behavior of median *CL* across any of the 40 distinct gaits, we turned to examining how *CL* varied locally along the length of the trackway for each trial condition, hence we developed a quality-of-fit measure.

The next step is to create a metric by which we can evaluate the variation in coupling length along the trackway for each trial, in order to find a 'best' solution.

Appendix 2

Evaluating quality of fit

We considered how *CL* varies along the trackway for each condition. We began by focusing on the *G2* walk gait (specifically *G2-1-60* and *G2-2-60*) and plotting their coupling length values versus cycle along the length of the trackway. Figure 17 shows the results for *G2-1-60* and *G2-2-60*, respectively, where the configuration *G2-2* has one additional stride length separation between the pes pair and the manus pair. Each of the following plots has a one-meter range on the ordinate centered on the median coupling length value for that trial. The observed variations in coupling length values along each trial arise from two potential sources. The first is noise, which is inherent in any biological system. The second is a characteristic perturbation to *CL* in response to the track pattern perturbation. It's this second type of characteristic variation that we will exploit, provided it can be distinguished from the noise.

With reference to Fig. 17, there are clear differences between the responses of the *G2-1-60* and the longer-coupled *G2-2-60* to this trackway. Since we hold constant both the gait and the duty factor, the difference between the two trials is essentially the 'body length' (by adding one stride length to the choice of manus tracks to associate with the given pes tracks). We seek to establish parameters derived from the coupling lengths in each trial that can be used to quantify the characteristic variations between trials. These parameters will form a "feature space" (a set of possible combinations of parameter values) that can be used to determine the fitness of each simulation trial as a solution for the trackway. However, as with many complex systems, the characteristic variations are not perfectly orthogonal to the noise. A feature space cannot be created that represents only the characteristic variations within trials. Some amount of noise will be included in each parameter and will have to be accounted for in the analysis using uncertainty and error propagation techniques.

What interpretation should be given to the variations in measured coupling length as it is applied along a trackway? This computation results from the application of fixed specific values for the free parameters to the positions of actual track locations. The irregularity in computed *CL* therefore results from the irregularity in the trackway, and even a trackway as subtly irregular as that in Fig. 7 could result in substantial variation in *CL*. This variation is difficult to explain in biological terms, as that would suggest the axial

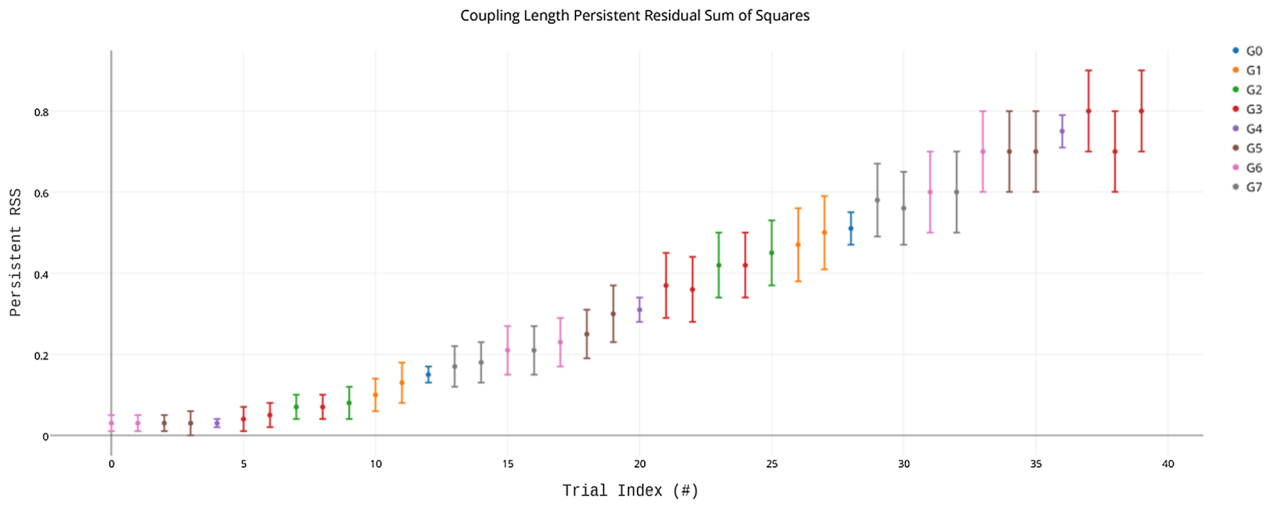

Fig. 19 *PRSS* values for the 40 trials of *CL* computations along BEB-500-S1

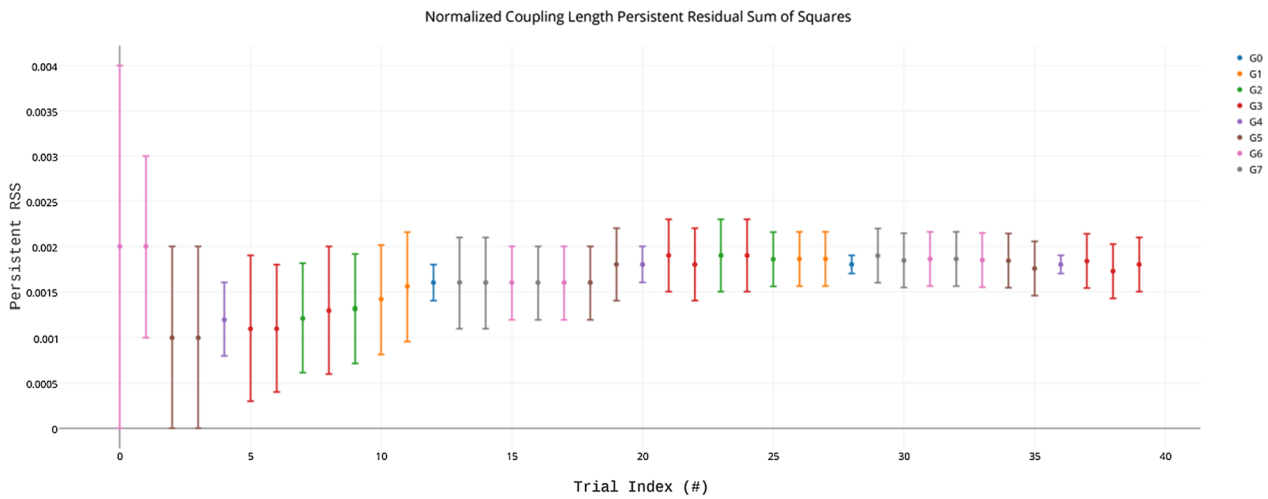

Fig. 20 *PRSS* values normalized to account for expected increases in *CL* across the different trial conditions

length of the trackmaker varied quite substantially during its passage. If we reject that conclusion, then it comes down to either having applied the 'wrong' choice of free parameters or having incorrectly assumed that the trackmaker walked with a constant gait as it created that trackway. To resolve this, we seek a metric on which to judge the suitability of a given gait as a model for the trackmaker's movements along an actual trackway. We do not seek to solve for the 'right' choice of gait parameters; rather we seek to rule out 'wrong' choices, based on a fitness function which we will develop.

Persistent residuals

Consider a fictional trackway where two simulation trials, *a* and *b*, produce coupling length plots with the same median value but rather different profiles (Fig. 18). We wish to quantify the salience of these differences.

A residual analysis is a common approach to distinguish these cases, wherein the difference between each sample and the expected value is calculated. Each difference is squared to make all values positive and to weigh relatively larger differences more strongly than smaller ones. If we specify the consistent baseline value as the

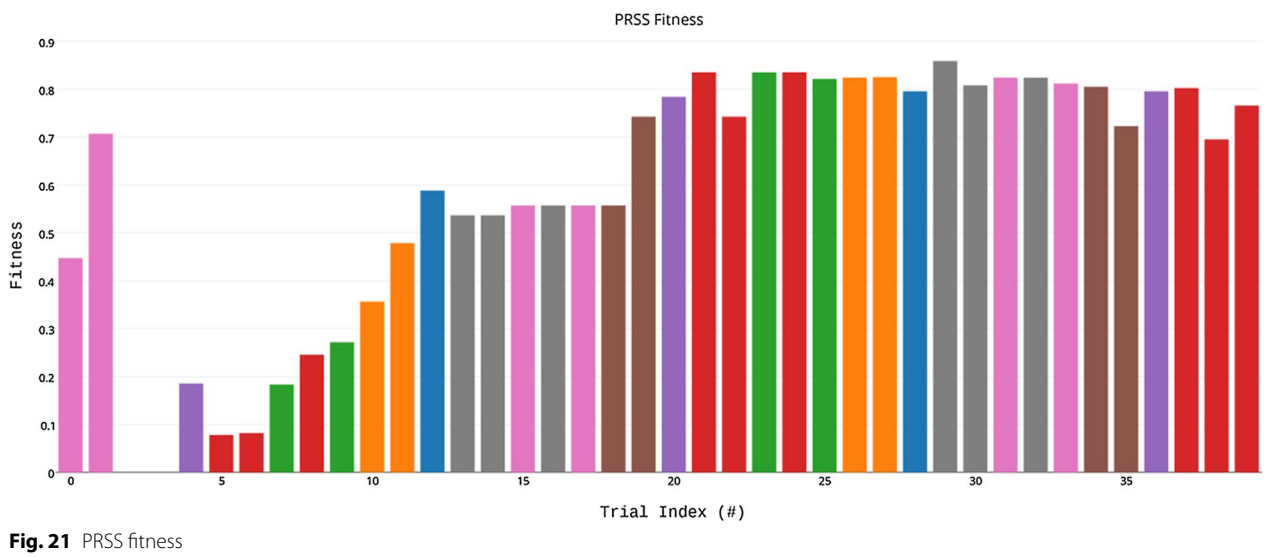

Fig. 21 PRSS fitness

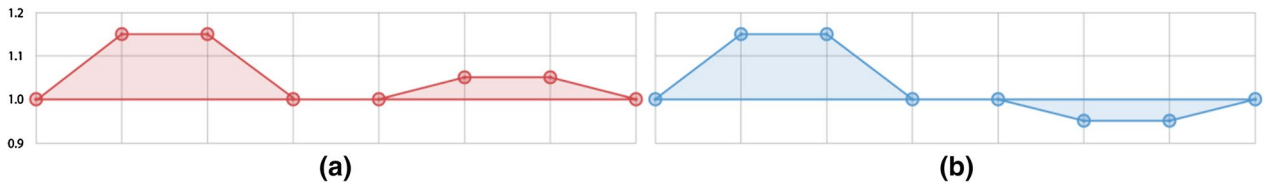

Fig. 22 In a, coupling length deviates from a median value at two separate points along the trackway with the same sign, while in b the deviations have opposite sign. Note that the area under the two curves is identical

expectation value, we can calculate this residual sum of the squares (*RSS*) as:

$$RSS = \sum_{i=1}^{N} (x_i - \overline{x})^2 \tag{8}$$

where $\overline{x}$ is the baseline value. For the two plots in Fig. 18, however, the *RSS* results are identical, hence a standard residual analysis would conclude that the two trials are equally efficacious solutions for that trackway.

We can improve the residual analysis by considering the physical restrictions on the trackmaker. In trial *a*, the two deviations are isolated and short in duration (consisting of one sample above the baseline in each case) while in trial *b* there is one deviation for twice the duration. Given we are computing coupling length along a trackway, one single step of either a pes or manus that deviates substantially from the median step length could produce an isolated deviation in *CL* from the baseline. A slightly longer (or shorter) than usual pes step at the same moment as a slightly shorter (or longer) manus step could also combine to create a short-isolated deviation in the *CL* computation. But the story is different for trial *b* in Fig. 18, where *CL* deviates from the baseline for two successive measurements. For the trackmaker to sustain a deviation from baseline for two or more successive measurements (one step cycle or more) requires some change in gait parameters, if one is to believe the trackmaker cannot substantially change its axial length during that protracted interval. Taking this into account requires altering the way the residuals are calculated. Our concern is not that a residual exists, but that a residual persists for a longer interval than would reflect an isolated deviation of the trackmaker. We can define this notion of persistence by replacing the square of each residual in the RSS calculation (Eq. 8) with the product of nearest neighbor residuals, i.e.,

$$PRSS = \sum_{i=1}^{N-1} |x_i - \overline{x}||x_{i+1} - \overline{x}| \tag{9}$$

Applied to our examples in Fig. 18, trial *a* has a value of $PRSS = 0$ while trial *b* has a $PRSS = 0.023$. The persistent residual effectively removes noise variations caused by single-sample deviations. With it we can conclude that trial *a* is a more efficacious solution for the trackway. In the example above we specified a reasonable, but somewhat arbitrary, value for the expectation value $\underline{x}$. For more general simulation trials, *PRSS* is better expressed as:

$$PRSS = \sum_{i=1}^{N-1} \left|CL_i - \overline{CL}\right|\left|CL_{i+1} - \overline{CL}\right| \tag{10}$$

where $\overline{CL}$ is the median length across the given simulation trial. Applying this *PRSS* formulation (Eq. 10) to the BEB-500 S1 trackway yields the following plot of the persistent residual sum of squares for coupling length (Fig. 19).

It is apparent that there is a scaling issue in these results. We did not observe this in our fictional example because the two trials shared the same expectation (baseline) values. Median coupling values generally differ in actual

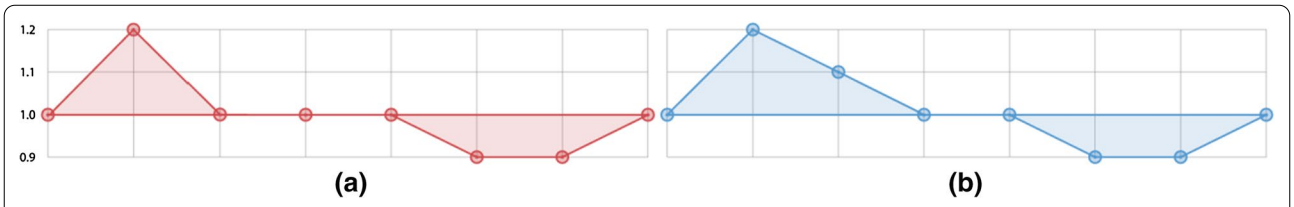

Fig. 23 The results of the two trials are identical but for the third sample, which is above baseline in *b*

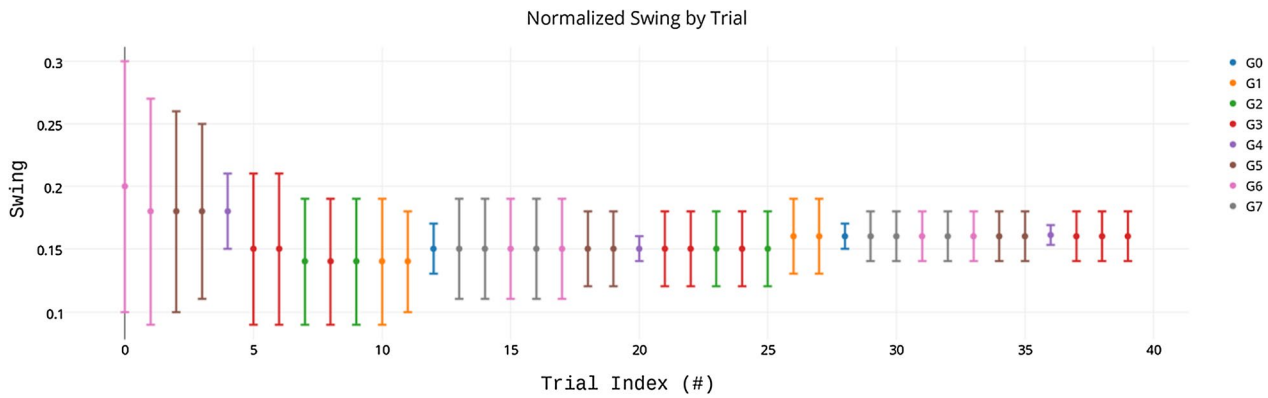

Fig. 24 Normalized swing by trial

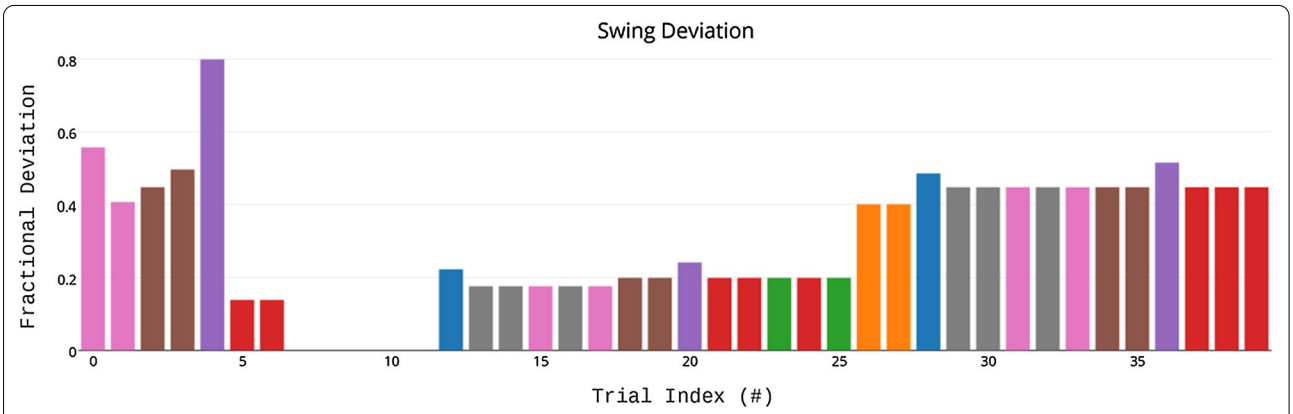

Fig. 25 The results of the swing deviation

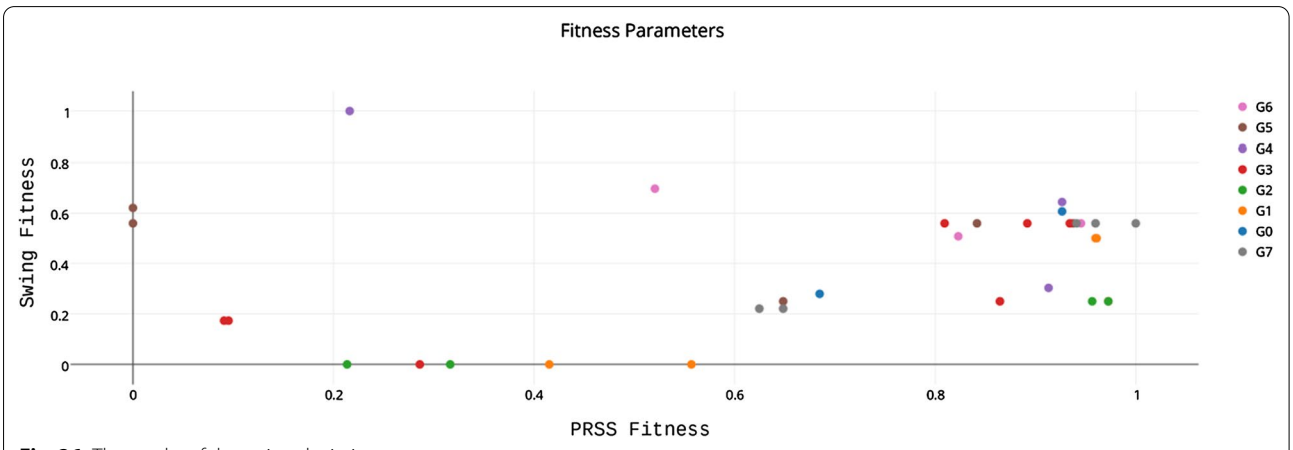

Fig. 26 The results of the swing deviation

simulation trials, however. Normalizing the residuals by their median coupling values eliminates the problem:

$$PRSS = \sum_{i=1}^{N-1} \left| \frac{CL_i}{\overline{CL}} - 1 \right| \left| \frac{CL_{i+1}}{\overline{CL}} - 1 \right| \tag{11}$$

There is another subtle issue caused by boundary conditions at the beginning and end of the trackway. The number of samples, *N*, in a trial depends on the gait for a given trial. For example, manus locators in a long-coupled trial (such as *G2-2*) are further ahead in a trackway than in a short-coupled trial (*G2-1*) at the same moment in a simulation, and therefore will complete fewer samples. This relatively penalizes those simulation trials with more samples, which is resolved by simply dividing the *PRSS* by the number of residuals in the summation:

$$PRSS = \frac{1}{N-1}\sum_{i=1}^{N-1}\left|\frac{CL_i}{\overline{CL}} - 1\right|\left|\frac{CL_{i+1}}{\overline{CL}} - 1\right| \tag{12}$$

PRSS can now be calculated by Eq. 12 for every simulation trial on a trackway and used to compare one trial to another. For BEB-500 S1 this yields the graph in Fig. 20.

We can now use *PRSS* values to compare the solution efficacy of the two trials *a* and *b* in terms of standard deviations:

$$\Delta PRSS = \frac{|PRSS_a - PRSS_b|}{\sqrt{\sigma_a^2 + \sigma_b^2}}, \tag{13}$$

where $\sigma_{(a,b)}$ are the uncertainties for the *a* and *b* trials.

While pairwise comparisons are useful, a global comparison across all trials would be preferable and allow the solution efficacy of every trial to be ranked at once. We therefore generalize the previous pairwise comparison formula (Eq. 13) to:

$$\Delta PRSS = \frac{|PRSS_i - PRSS_{\min}|}{\sqrt{\sigma_i^2 + \sigma_{\min}^2}} \tag{14}$$

Comparisons are made for each trial relative to the smallest persistent residual sum-of-squares value, $PRSS_{min}$, from the collection of solutions. A value of 0 indicates that there is no observed difference between a particular trial and the 'best' solution while values greater than 0 indicate a less efficacious solution than $PRSS_{min}$. This makes Δ_{PRSS} suitable as a fitness parameter for persistent residuals (Fig. 21).

Swing

Consider another fictional trackway where this time two simulation trials *a* and *b* produce the two coupling length *CL* plots in Fig. 22. Each trial has two persistent deviation regions, one large and one small. While the two persistent deviation regions are both positive in trial *a*, in trial *b* they swing from positive to negative.

The value of *PRSS* for these two trials is 0.025 and thus fails to distinguish the differences in the sign of the residuals, which represents a greater range of *CL* values for trial *b* than trial *a*. Another parameter is therefore needed to express the overall range of coupling length values within a trial. We define this parameter, which we will call swing, as the difference between the minimum and maximum coupling length values:

$$swing = \frac{|CL_{\max} - CL_{\min}|}{CL_{median}} \tag{15}$$

It is normalized by the median coupling length value in order to avoid the scaling issue that arose earlier in the PRSS formulation when comparing trials with different median coupling lengths. For trials *a* and *b* in Fig. 22 the calculated swing values are 0.15 and 0.2, respectively. The smaller swing for trial *a* suggests that *a* is a better solution than trial *b* (i.e., the trackmaker using gait *a* would have had a lesser transient deviation from steady state than if using gait *b*).

But the swing formulation is not yet complete. We previously established the importance of persistence in the formulation of the *PRSS* parameter. Persistence pertains to swing as well. While deviation for the course of one sample can be attributed to noise, deviation for more samples likely indicates more than noise as the underlying cause. To illustrate this, suppose another fictional trackway produced the following two coupling length plots for two trials *a* and *b* (Fig. 23).

In this example, the only difference between trials *a* and *b* is the third coupling length sample, which, in Fig. 23a has zero deviation from the baseline value, while in Fig. 23b that sample has a non-zero deviation from the baseline value. Using the formulation for swing outlined above, these two example trials have the same swing value despite the greater persistence of a deviation in trial *b* than in trial *a*. This is efficiently resolved by introducing a forward-moving average, which is generally defined in the form

$$\bar{x}_i = \frac{x_i + x_{i+1}}{2} \tag{16}$$

Next, we need to incorporate the uncertainties of the samples into this forward-moving average, resulting in a weighted version:

$$\overline{CL}_i = \frac{\frac{CL_i}{\sigma_i^2} + \frac{CL_{i+1}}{\sigma_{i+1}^2}}{\sigma_i + \sigma_{i+1}} \tag{17}$$

where σ_i and σ_{i+1} are the uncertainties in coupling length values at i and i+1. The weighted averaged coupling length values can then be substituted into the previous swing Eq. (15) as

$$swing = \frac{\left|\overline{CL}_{\max} - \overline{CL}_{\min}\right|}{CL_{median}} \tag{18}$$

This updated swing formulation now properly distinguishes between the two trials from the previous example with a higher swing value for trial *b* than for trial *a*. Applying this swing formulation (Eq. 18) to BEB-500 S1 yields the plot in Fig. 24.

In the same fashion as the *PRSS* parameter, the swing parameter needs to be converted into a fitness parameter for comparison across trials. We use the same approach for swing as we used for PRSS. That is, the lowest swing value among the trials is used as the highest fitness value, and all other trials are compared to it using the deviation significance calculation:

$$\Delta_{swing} = \frac{\left|swing_i - swing_{\min}\right|}{\sqrt{\sigma_i^2 + \sigma_{\min}^2}} \tag{19}$$

The computed swing deviation is shown in Fig. 25.

Solution fitness

Now that we have our two fitness parameters Δ_{PRSS} and Δ_{swing} (Eqs. 14 and 19) we combine them by plotting each trial on a scatter plot with the parameters as the values for each axis. To weigh the fitness parameters equally, the values for all of the trials are rescaled to a maximum of 1 (Fig. 26).

The closer a particular trial is to the origin of this fitness parameter space, the more efficacious a solution the trial is for the trackway. Computing the Euclidean distance for each point creates the final fitness parameter ranking for the trials

$$fitness = \sqrt{\Delta_{swing}^2 + \Delta_{PRSS}^2} \tag{20}$$

And finally, to more clearly present the quality-of-fitness, the fitness for each trial is subtracted from the poorest fitness to yield the plot in Fig. 11.

Acknowledgements
We gratefully acknowledge the funding by the Swiss Federal Roads Office and Canton Jura, and the Office de la culture—Paléontologie A16. Excavations and scientific documentation of Highway A16 dinosaur tracksites and related research by the Paléontologie A16 (Section d'Archéologie et Paléontologie, Office de la culture) were funded by the Swiss Federal Roads Office (FEDRO, 95%) and the Canton Jura (5%), and this important funding is acknowledged very much indeed. We thank all technicians, photographers, geometers, drawers, collection managers, and preparators involved during the excavation and documentation of the tracksites. We greatly appreciate the suggestions of the two anonymous reviewers.

Author contributions
DM and the Office de la culture documented the extensive trackway assemblages of the A16 Highway project by site maps, spreadsheets, and photographs. SE developed the framework that led from those documents to a database from which selected trackway segments could be analyzed in this study. SE developed the theoretical and probabilistic analyses of the Coupling Length model. KAS developed 3D graphics software to interactively populate this database with track measurements (plus quantified uncertainty estimates), mapping over 6000 sauropod tracks from the site maps and photographs. The three authors collaborated equally to refine the process of track and trackway measurement uncertainty, the selection of trackway segments for analysis, and confirmation of measurements and uncertainties with reference to the original material. KAS and SE shared in the writing and illustrating the paper. All authors read and approved the final manuscript.

Funding
This research was supported by the Swiss Federal Roads Office and Canton Jura, and the Office de la culture—Paléontologie A16. Excavations and scientific documentation of Highway A16 dinosaur tracksites and related research by the Paléontologie A16 (Section d'Archéologie et Paléontologie, Office de la culture) were funded by the Swiss Federal Roads Office (FEDRO, 95%) and the Canton Jura (5%).

Availability of data and materials
The trackway data is available in its entirety in the Final Report "Statistical analyses of Highway A16 dinosaur trackways" by Kent A. Stevens and Scott Ernst, Office de la culture, Porrentruy, Canton Jura, CH. The datasets used for the current study are available from the corresponding author.

Declarations

Ethics approval and consent to participate
Not applicable.

Consent for publication
Not applicable.

Competing interests
The authors declare that they have competing interests.

Author details
[1]Department of Computer and Information Science, University of Oregon, Eugene, OR 97403, USA. [2]Maple Grove, USA. [3]Naturhistorisches Museum Basel, Augustinergasse 2, 4051 Basel, Switzerland.

Received: 22 September 2021 Accepted: 26 March 2022
Published online: 12 May 2022

References

Alexander, R. M. (1976). Estimates of speeds of dinosaurs. *Nature, 261*, 129–130.
Belvedere, M. (2008). *Ichnological researches on the Upper Jurassic dinosaur tracks in the Iouaridène area (Demnat, Central High-Atlas, Morocco) Ph.D. Thesis* (p. 121). Università degli Studi di Padova.
Biewener, A. A. (1983). Allometry of quadrupedal locomotion: The scaling of duty factor, limb curvature and limb orientation to body size. *Journal of Experimental Biology, 105*, 147–171.
Biknevicius, A. R., & Reilly, S. M. (2006). Correlation of symmetrical gaits and whole body mechanics: Debunking myths in locomotor biodynamics. *Journal of Experimental Zoology, 305A*, 923–934.
Bonnan, M. F. (2005). Pes anatomy in sauropod dinosaurs: Implications for functional morphology, evolution, and phylogeny. In K. Carpenter & V. Tidwell (Eds.), *Thunder-lizards: The sauropodomorph dinosaurs* (pp. 346–380). Indiana University Press.
Bonnan, M. F., Sandrik, J. L., Nishiwaki, T., Wilhite, D. R., Elsey, R. M., & Vittore, C. (2010). Calcified cartilage shape in archosaur long bones reflects overlying joint shape in stress-bearing elements: Implications for nonavian dinosaur locomotion. *The Anatomical Record: Advances in*

Integrative Anatomy and Evolutionary Biology, 293, 2044–2055. https://doi.org/10.1002/ar.21266
Bonnan, M. F., Shulman, J., Varadharajan, R., Gilbert, C., Wilkes, M., Horner, A., & Brainerd, E. (2016). Forelimb kinematics of rats using XROMM, with implications for small eutherians and their fossil relatives. *PLoS ONE, 11*(3), e0149377.
Casanovas, M., Fernández, A., Pérez-Lorente, F., & Santafé, J. V. (1997). Sauropod trackways from site El Sobaquillo (Munilla, La Rioja, Spain) indicate amble walking. *Ichnos: an International Journal of Plant & Animal, 5*(2), 101–107. https://doi.org/10.1080/10420949709386409
Cavagna, G. A., Heglund, N. C., & Taylor, C. R. (1977). Mechanical work in terrestrial locomotion: Two basic mechanisms for minimizing energy expenditure. *American Journal of Physiology, 233*, 243–261.
Demathieu, G. R. (1970). *Les empreintes de pas de vertébrés du Trias de la bordure nord-est du Massif Central* (p. 211). Cahiers de Paléontologie, Éditions du Centre National de la Recherche Scientifique.
Farlow, J. O., Pittman, J. G., & Hawthorne, J. M. (1989). *Brontopodus birdi*, lower cretaceous sauropod footprints from the U.S. Gulf Coastal Plain. In D. D. Gillette & M. G. Lockley (Eds.), *Dinosaur tracks and traces* (pp. 371–394). Cambridge University Press.
Fischer, M. S., Schilling, N., Schmidt, M., Haarhaus, D., & Witte, H. (2002). Basic limb kinematics of small therian mammals. *Journal of Experimental Biology, 205*(9), 1315–1338.
Gallup, M. A. (1989). Functional morphology of the hindfoot of the Texas sauropod *Pleurocoelus* sp. indet. Paleobiology of the Dinosaurs. *Geological Society of America Special Paper, 238*, 71–74.
Gambaryan, P. P. (1974). *How animals run* (p. 365). Wiley.
Genin, J. J., Willems, P. A., Cavagna, G. A., Lair, R., & Heglund, N. C. (2010). Biomechanics of locomotion in Asian elephants. *Journal of Experimental Biology, 213*(5), 694–706.
González Riga, B. J. (2011). Speeds and stance of titanosaur sauropods: Analysis of *Titanopodus* tracks from the Late Cretaceous of Mendoza, Argentina. *Annals of the Brazilian Academy of Sciences, 83*, 1–12.
González Riga, B. J., & Tomaselli, M. B. (2019). Different trackway patterns in titanosaur sauropods: Analysis of new *Titanopodus* tracks from the Upper Cretaceous of Mendoza, Neuquén Basin, Argentina. *Cretaceous Research, 93*, 49–59.
Griffin, T. M., Main, R. P., & Farley, C. T. (2004). Biomechanics of quadrupedal walking: How do four-legged animals achieve inverted pendulum-like movements? *Journal of Experimental Biology, 207*, 3545–3558.
Halfpenny, J. C. (1987). *A field guide to mammal tracking in North America* (2nd ed., p. 176). Johnson Books.
Hildebrand, M. (1965). Symmetrical gaits of horses. *Science, 150*, 701–708.
Hildebrand, M. (1976). Analysis of tetrapod gaits: General considerations and symmetrical gaits. In R. M. Herman, S. Grillner, P. S. G. Stein, & D. G. Stuart (Eds.), *Neural control of locomotion* (pp. 203–236). Plenum.
Hildebrand, M. (1989). The quadrupedal gaits of vertebrates. *BioScience, 39*(11), 766–775.
Holliday, C. M., Ridgely, R. C., Sedlmayr, J. C., & Witmer, L. M. (2010). Cartilaginous epiphyses in extant archosaurs and their implications for reconstructing limb function in dinosaurs. *PLoS ONE, 5*, e13120.
Hutchinson, J. R., Famini, D., Lair, R., & Kram, R. (2003). Biomechanics: Are fast-moving elephants really running? *Nature, 422*, 493–494.
Hutchinson, J. R., Schwerda, D., Famini, D., Dale, R. H. I., Fischer, M., & Kram, R. (2006). The locomotor kinematics of African and Asian elephants: Changes with speed and size. *Journal of Experimental Biology, 209*, 3812–3827.
Irschick, D. J., & Jayne, B. C. (1999). Comparative three-dimensional kinematics of the hindlimb for high-speed bipedal and quadrupedal locomotion of lizards. *Journal of Experimental Biology, 202*(9), 1047–1065.
Ishigaki, S. (1988). Les empreintes de dinosaures du Jurassique inférieur du Haut Atlas Central marrocain. *Notes Service Geologuique Du Maroc, 44*, 79–96.
Lammers, A. R., & Biknevicius, A. R. (2004). The biodynamics of arboreal locomotion: The effects of substrate diameter on locomotor kinetics in the gray short-tailed opossum (*Monodelphis domestica*). *Journal of Experimental Biology, 207*, 4325–4336.
Leonardi, G. (1987). *Glossary and manual of tetrapod footprint palaeoichnology* (p. 117). Publicação do Departemento Nacional da Produção Mineral Brasil.
Lockley, M. G. (1991). *Tracking Dinosaurs: A new look at an ancient world* (p. 238). Cambridge University Press.
Lovelace, D. M., Hartman, S. A., & Wahl, W. R. (2007). Morphology of a specimen of *Supersaurus* (Dinosauria, Sauropoda) from the Morrison Formation of Wyoming, and a re-evaluation of diplodocid phylogeny. *Arquivos Do Museu Nacional, Rio De Janeiro, 65*(4), 527–544.
Marty, D. (2008). Sedimentology, taphonomy, and ichnology of Late Jurassic dinosaur tracks from the Jura carbonate platform (Chevenez-Combe Ronde tracksite, NW Switzerland): Insights into the tidal-flat palaeoenvironment and dinosaur diversity, locomotion, and palaeoecology. *GeoFocus, 21*, 1–278.
Marty, D., Ayer, J., Becker, D., Berger, J.-P., Billon-Bruyat, J.-P., Braillard, L., Hug, W. A., & Meyer, C. A. (2007). Late Jurassic dinosaur tracksites of the Transjurane highway (Canton Jura, NW Switzerland): Overview and measures for their protection and valorization. *Bulletin for Applied Geology, 12*, 75–89.
Marty, D., Cavin, L., Hug, W. A., Jordan, P., Lockley, M. G., & Meyer, C. A. (2004). The protection, conservation and sustainable use of the Courtedoux dinosaur tracksite, Canton Jura, Switzerland. *Revue De Paléobiologie, 9*, 39–49.
Marty, D., Hug, W. A., Iberg, A., Cavin, L., Meyer, C. A., et al. (2003). Preliminary report on the Courtedoux dinosaur tracksite from the Kimmeridgian of Switzerland. *Ichnos, 10*, 209–219.
Marty, D., Paratte, G., Lovis, C., Jacquemet, M., & Meyer, C. A. (2010). *Extraordinary sauropod trackways from the Late Jurassic Béchat Bovais tracksite (Canton Jura, NW Switzerland): Implications for sauropod locomotor styles* (p. 56). 8th Annual Meeting of the European Association of Vertebrate Palaeontologists.
Mazzetta, G. V., & Blanco, R. E. (2001). Speeds of dinosaurs from the Albian-Cenomanian of Patagonia and sauropod stance and gait. *Acta Palaeontologica Polonica, 46*, 235–246.
Padian, K., & Olsen, P. E. (1984). Footprints of the Komodo monitor and the trackways of fossil reptiles. *Copeia, 1984*, 662–671.
Paratte, G., Lapaire, M., Lovis, C., & Marty, D. (2018). *Traces de dinosaures jurassiques Contexte et méthode (Catalogues du patrimoine paléontologique jurassien—A16)*. Office de la culture—Paléontologie A16.
Peabody, F. E. (1959). Trackways of living and fossil salamanders. *Univ Calif Publ Zool, 63*, 1–72.
Platt, B. F., & Hasiotis, S. T. (2006). Newly discovered sauropod dinosaur tracks with skin and foot-pad impressions from the Upper Jurassic Morrison Formation, Bighorn Basin, Wyoming, USA. *Palaios, 21*(3), 249–261.
Reilly, S. M., & Biknevicius, A. R. (2003). Integrating kinetic and kinematic approaches to the analysis of terrestrial locomotion. In V. L. Bels, J. P. Gasc, & A. Casinos (Eds.), *Vertebrate biomechanics and evolution* (pp. 243–265). Bios Scientific Publishers Ltd.
Schmitt, D., Cartmill, M., Griffin, T. M., Hanna, J. B., & Lemelin, P. (2006). Adaptive value of ambling gaits in primates and other mammals. *Journal of Experimental Biology, 209*(11), 2042–2049.
Schwarz, D., Ikejiri, T., Breithaupt, B. H., Sander, P. M., & Klein, N. (2007). A nearly complete skeleton of an early juvenile diplodocid (Dinosauria: Sauropoda) from the Lower Morrison Formation (Late Jurassic) of North Central Wyoming and its implications for early ontogeny and pneumaticity in sauropods. *Historical Biology, 19*, 225–253.
Schwarz, D., Wings, O., & Meyer, C. A. (2007). Super sizing the giants: First cartilage preservation at a sauropod dinosaur limb joint. *Journal of the Geological Society, London, 164*, 61–65.
Stevens, K. A. (2013). The articulation of sauropod necks: Methodology and mythology. *PLoS ONE, 8*(10), e78572.
Stevens, K. A., & Ernst, S. (2017). *Statistical analyses of highway A16 dinosaur trackways: Final report* (p. 5895). Paléontologie A16 Étude Intermédiaire 81.
Stevens, K. A., Ernst, S., & Marty, D. (2016). Uncertainty and ambiguity in the interpretation of sauropod trackways. In P. L. Falkingham, D. Marty, & A. Richter (Eds.), *Dinosaur tracks. The next steps* (pp. 227–243). Indiana University Press.
Stevens, K. A., Ernst, S., & Marty, D. (2017). The importance of being uncertain: Probabilistic computation of trackmaker size, gait and gauge. *Meeting program and abstracts* (p. 198). Society of Vertebrate Paleontology 77th annual Meeting.

Taylor, J. (1997). *Introduction to error analysis, the study of uncertainties in physical measurements* (2nd ed., p. 327). University Science Books.
Thulborn, R. A. (1990). *Dinosaur tracks* (p. 410). Chapman & Hall.
Tschopp, E., Wings, O., Frauenfelder, T., & Brinkmann, W. (2015). Articulated bone sets of manus and pedes of *Camarasaurus* (Sauropoda, Dinosauria). *Palaeontologia Electronica*. https://doi.org/10.26879/559
Vila, B., Oms, O., Galobart, À., Bates, K. T., Egerton, V. M., et al. (2013). Dynamic similarity in titanosaur sauropods: Ichnological evidence from the fumanya dinosaur tracksite (Southern Pyrenees). *PLoS ONE, 8*(2), e57408. https://doi.org/10.1371/journal.pone.0057408
Wilhite, R. D. (2005). Variation in the appendicular skeleton of North American sauropod dinosaurs: Taxonomic implications. In K. Carpenter & V. Tidwell (Eds.), *Thunder-lizards: The sauropodomorph dinosaurs* (pp. 268–301). Indiana University Press.
Wimberly, A. N., Slater, G. J., & Granatosky, M. C. (2021). Evolutionary history of quadrupedal walking gaits shows mammalian release from locomotor constraint. *Proceedings of the Royal Society B, 288*, 20210937. https://doi.org/10.1098/rspb.2021.0937
Woodruff, D. C., Carr, T. D., Storrs, G. W., Waskow, K., Scannella, J. B., Nordén, K. K., & Wilson, J. P. (2018). The smallest diplodocid skull reveals cranial ontogeny and growth-related dietary changes in the largest dinosaurs. *Scientific Reports, 8*(1), 1–12.
Woodruff, D. C., & Foster, J. R. (2017). The first specimen of *Camarasaurus* (Dinosauria: Sauropoda) from Montana: The northernmost occurrence of the genus. *PLoS ONE, 12*(5), e0177423.
Zips, S., Peham, C., Scheidl, M., Licka, T., & Girtler, D. (2001). Motion pattern of the toelt of Icelandic horses at different speeds. *Equine Veterinary Journal, 33*, 109–111.

Publisher's Note